iScience

CellPress

Article

Serine Phosphorylation by mTORC1 Promotes IRS-1 Degradation through SCFβ-TRCP E3 Ubiquitin Ligase

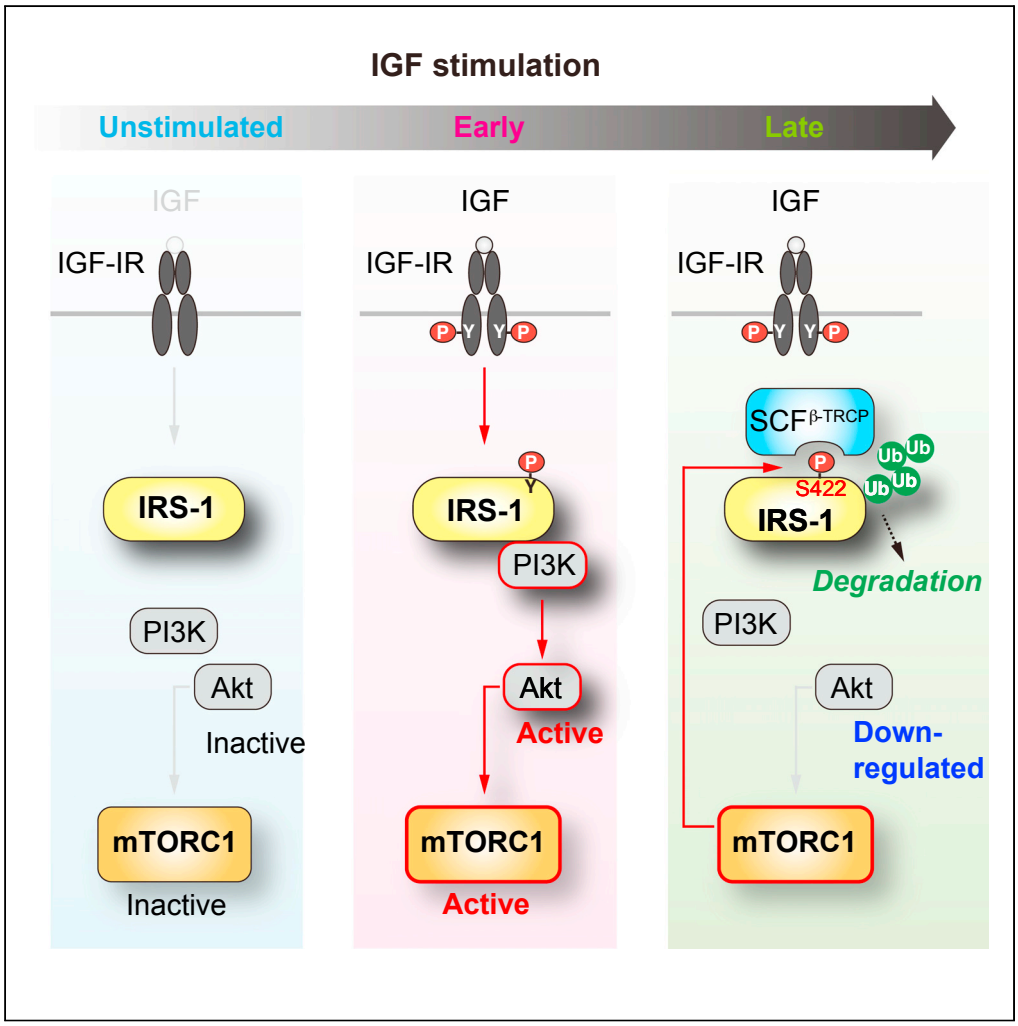

Yosuke Yoneyama, Tomomi Inamitsu, Kazuhiro Chida, ..., Tatsuya Maeda, Fumihiko Hakuno, Shin-Ichiro Takahashi

atkshin@mail.ecc.u-tokyo.ac.jp

HIGHLIGHTS

Ser 422 of IRS-1 is identified as a phosphorylation site by mTORC1

Phosphorylation of Ser 422 induces the binding of SCF β-TRCP E3 ligase to IRS-1

Ser 422 phosphorylation triggers the SCF β-TRCP-mediated degradation of IRS-1

The IRS-1-mTORC1 negative feedback loop determines the duration of IGF signaling

Yoneyama et al., iScience 5, 1–18
July 27, 2018
https://doi.org/10.1016/j.isci.2018.06.006

iScience

CellPress

Article

Serine Phosphorylation by mTORC1 Promotes IRS-1 Degradation through SCFβ-TRCP E3 Ubiquitin Ligase

Yosuke Yoneyama,[1,6] Tomomi Inamitsu,[1] Kazuhiro Chida,[1] Shun-Ichiro Iemura,[2] Tohru Natsume,[3] Tatsuya Maeda,[4,5] Fumihiko Hakuno,[1] and Shin-Ichiro Takahashi[1,7,*]

SUMMARY

The insulin receptor substrate IRS-1 is a key substrate of insulin and insulin-like growth factor (IGF) receptor tyrosine kinases that mediates their metabolic and growth-promoting actions. Proteasomal degradation of IRS-1 is induced following activation of the downstream kinase mTOR complex 1 (mTORC1) to constitute a negative feedback loop. However, the underlying mechanism remains poorly understood. Here we report that Ser 422 of IRS-1 is phosphorylated by mTORC1 and required for IRS-1 degradation induced by prolonged IGF stimulation. Phosphorylation of Ser 422 then recruits the $SCF^{\beta\text{-}TRCP}$ E3 ligase complex, which catalyzes IRS-1 ubiquitination. Phosphorylation-dependent IRS-1 degradation contributes to impaired growth and survival responses to IGF in cells lacking TSC2, a negative regulator of mTORC1. Inhibition of IRS-1 degradation promotes sustained Akt activation in IGF-stimulated cells. Our work clarifies the nature of the IRS-1-mTORC1 feedback loop and elucidates its role in temporal regulation of IGF signaling.

INTRODUCTION

Insulin and insulin-like growth factors (IGFs), IGF-I and IGF-II, play pivotal roles in growth, differentiation, survival, and various aspects of metabolism in a wide range of mammalian tissues (Nakae et al., 2001). Upon ligand binding, activated insulin/IGF-I receptors phosphorylate a family of insulin receptor substrate (IRS) proteins (White, 2002). Tyr-phosphorylated IRS proteins provide docking sites for the class I phosphatidylinositol 3-kinase (PI3K) (Myers et al., 1996; Sun et al., 1993), which generates phosphatidylinositol-3,4,5-triphosphate leading to activation of the Ser/Thr kinase Akt (Manning and Cantley, 2007). Akt is primarily responsible for the ability of insulin and IGFs to stimulate cell growth, survival, differentiation, and metabolic responses.

Among downstream kinases in insulin/IGF signaling, the Ser/Thr kinase mechanistic target of rapamycin (mTOR) regulates many activities of insulin/IGF. mTOR functions as the core catalytic component of two structurally and functionally distinct complexes, mTORC1 and mTORC2 (Saxton and Sabatini, 2017). mTORC2 is primarily involved in the PI3K/Akt pathway where upon PI3K activation, PDK1 and mTORC2 phosphorylate Thr 308 and Ser 473 of Akt, respectively, and activate it. mTORC1 phosphorylates distinct substrates, including S6 kinase 1 (S6K1) and the eukaryotic translation initiation factor 4E binding protein 1/2 (4EBP1/2) (Ma and Blenis, 2009), to regulate protein translation, autophagy, and cell growth. In cells stimulated with growth factors, Akt activates mTORC1 by phosphorylation-mediated suppression of the tuberous sclerosis complex (TSC) protein complex, which inhibits the small GTPase Rheb, an essential activator of mTORC1 (Inoki et al., 2002; Manning et al., 2002; Menon et al., 2014).

Downstream kinases, including mTOR, phosphorylate multiple Ser/Thr residues of IRS proteins, which affects the signaling ability of IRS (Copps and White, 2012). Importantly, multiple Ser/Thr phosphorylations and subsequent proteasomal degradation of IRS-1, a major IRS family protein, are induced by prolonged exposure to insulin or IGF in various types of cells, where Akt activity, initially stimulated by the ligands, then later decreases (Haruta et al., 2000; Kim et al., 2012; Shi et al., 2011; Yoneyama et al., 2018), suggesting that IRS-1 degradation acts as an intrinsic feedback inhibition mechanism in the PI3K/Akt signaling. The IRS-1 degradation is sensitive to rapamycin (Berg et al., 2002; Hartley and Cooper, 2002; Haruta et al., 2000; Kim et al., 2012; Lee et al., 2000; Yoneyama et al., 2018). In addition, forced activation of mTORC1 results in IRS-1 degradation (Harrington et al., 2004; Shah et al., 2004), indicating that feedback phosphorylation of IRS-1 by the mTORC1/S6K cascade underlies IRS-1 degradation caused by persistent ligand stimulation.

[1]Department of Animal Resource Sciences and Applied Biological Chemistry, Graduate School of Agriculture and Life Sciences, The University of Tokyo, Bunkyo-ku, Tokyo 113-8657, Japan

[2]Translational Research Center, Fukushima Medical University, Fukushima-city, Fukushima 960-8031, Japan

[3]Molecular Profiling Research Center for Drug Discovery (molprof), National Institute of Advanced Industrial Science and Technology (AIST), Koto-ku, Tokyo 135-0064, Japan

[4]Institute for Quantitative Biosciences, The University of Tokyo, Bunkyo-ku, Tokyo 113-0032, Japan

[5]Department of Integrated Human Sciences, Faculty of Medicine, Hamamatsu University School of Medicine, Hamamatsu-city, Shizuoka 431-3192, Japan

[6]Present address: Institute of Research, Tokyo Medical and Dental University, 1-5-45 Yushima, Bunkyo-ku, Tokyo 113-8510, Japan

[7]Lead Contact

*Correspondence: atkshin@mail.ecc.u-tokyo.ac.jp

https://doi.org/10.1016/j.isci.2018.06.006

Although several distinct E3 ubiquitin ligases have been reported to ubiquitinate IRS-1, including SOCS1/3, Cbl-b, Mdm2, MG53, Cullin7-Fbxw8 complex, and SCF^{Fbxo40} complex (Nakao et al., 2009; Rui et al., 2002; Shi et al., 2011; Usui et al., 2004; Xu et al., 2008; Yi et al., 2013), the general mechanism underlying Ser/Thr phosphorylation-dependent degradation of IRS-1 remains elusive because of the complexity of IRS-1 Ser/Thr phosphorylation. In particular, the specific phosphorylated Ser/Thr residue(s) responsible for IRS-1 degradation stimulated by prolonged insulin/IGF exposure has not been identified.

Here we report that the $SCF^{\beta\text{-}TRCP}$ complex mediates mTORC1-induced degradation of IRS-1 in cells stimulated by prolonged IGF. In addition, we demonstrate that Ser 422 is a *bona fide* target phosphorylation site of mTORC1 and required for IRS-1 degradation and feedback inhibition of the PI3K/Akt signaling. Our work clarifies the nature of the mTORC1-IRS-1 feedback axis playing important roles in balancing IGF signaling and its activities.

RESULTS

Activation of mTORC1 Is Necessary and Sufficient to Induce IRS-1 Degradation

To elucidate the negative feedback mechanisms for degrading IRS-1, we used L6 myoblast cells in which IRS-1 critically contributes to IGF signaling and its bioactivities (Huang et al., 2005; Yoneyama et al., 2018, 2013). In the L6 cells, the phosphorylation of IRS-1, which was reflected by a mobility shift on SDS-PAGE, was observed 1 hr after IGF-I stimulation followed by the marked decrease in IRS-1 protein levels in the later period (6 hr) (Figure 1A). In contrast, IRS-2 levels were not largely affected by IGF-I. We confirmed that the decrease in IRS-1 levels observed after prolonged IGF-I stimulation was blocked by proteasomal inhibitors (Figure S1A). To explore Ser/Thr kinase(s) controlling IRS-1 degradation, we examined the IRS-1 abundance in IGF-I-stimulated cells pretreated with a panel of inhibitors against the mTOR pathway. Consistent with previous studies (Berg et al., 2002; Hartley and Cooper, 2002; Haruta et al., 2000; Kim et al., 2012), inhibition of mTOR with Torin1 and rapamycin blocked the degradation of IRS-1 induced by prolonged IGF-I stimulation (Figure 1A). Treatment with Torin1 and rapamycin also inhibited IGF-I-induced polyubiquitination of IRS-1, which was assessed by immunoprecipitation of FLAG-tagged IRS-1 (FLAG-IRS-1) under denaturing conditions (Figure 1B). In contrast, treatment with the S6K1 inhibitor, PF-4708671 (Pearce et al., 2010), did not affect the IRS-1 levels (Figure 1A), indicating the negligible role of S6K1 activity in IRS-1 degradation. We next evaluated the effects of the mTOR pathway inhibitors on Ser/Thr phosphorylation of IRS-1 by using site-specific phospho-IRS-1 antibodies. In L6 cells, IGF-I-induced phosphorylation of Ser 302, Ser 307, and Ser 318 was sensitive to Torin1 and rapamycin, whereas PF-470861 partially inhibited phosphorylation of Ser 302, but not of other Ser sites (Figure S1B). We also used mouse primary embryonic fibroblasts (MEFs) as another cell model to assess if the mTOR pathway is required for IRS-1 degradation. In MEFs, Torin1 treatment blocked the degradation of IRS-1 induced by IGF-I stimulation, whereas rapamycin partially did and PF-470861 did not (Figure S1C). These data suggest that mTOR activity is required for both multiple Ser phosphorylations and degradation of IRS-1 induced by IGF-I stimulation.

Previous studies have indicated that the IRS-1 level is markedly reduced in TSC1- and TSC2-deficient MEFs, which exhibit constitutively elevated mTORC1 signaling (Harrington et al., 2004; Shah et al., 2004). We generated TSC2 knockout L6 cells (L6 TSC2 KO cells) by using the CRISPR (clustered regularly interspaced short palindromic repeats)-Cas9 (CRISPR-associated protein 9) system (Figure S1D). Under both IGF-I-unstimulated and stimulated conditions, the IRS-1 levels were dramatically reduced in L6 TSC2 KO cells (Figure 1C). In addition, phosphorylation of Akt was insensitive to IGF-I in these cells, consistent with previous reports (Harrington et al., 2004; Shah et al., 2004). Under serum starvation conditions, treatment with Torin1 and rapamycin restored the IRS-1 levels comparable with those in wild-type cells, whereas treatment with PF-470861 had minor effects (Figure 1D). Thus, activation of mTORC1 is necessary and sufficient to induce IRS-1 degradation.

Cullin1 and β-TRCP1/2 Are Required for IRS-1 Degradation Induced by Prolonged IGF Stimulation

Several RING-type E3 ligases have been reported to ubiquitinate IRS-1 (Nakao et al., 2009; Rui et al., 2002; Shi et al., 2011; Usui et al., 2004; Xu et al., 2008; Yi et al., 2013). We co-expressed IRS-1 together with these E3 ligases or their subunits in 293T cells and analyzed the interaction by co-immunoprecipitation. Among them, Cullin1 strongly bound to IRS-1 (Figure 2A). In addition, small interfering RNA (siRNA)-mediated knockdown of Cullin1, but not of Cullin7 or Fbxw8, significantly inhibited the degradation of IRS-1 induced by prolonged IGF-I stimulation (Figures 2B and S2A), indicating that Cullin1 is required for IGF-I-induced degradation of IRS-1.

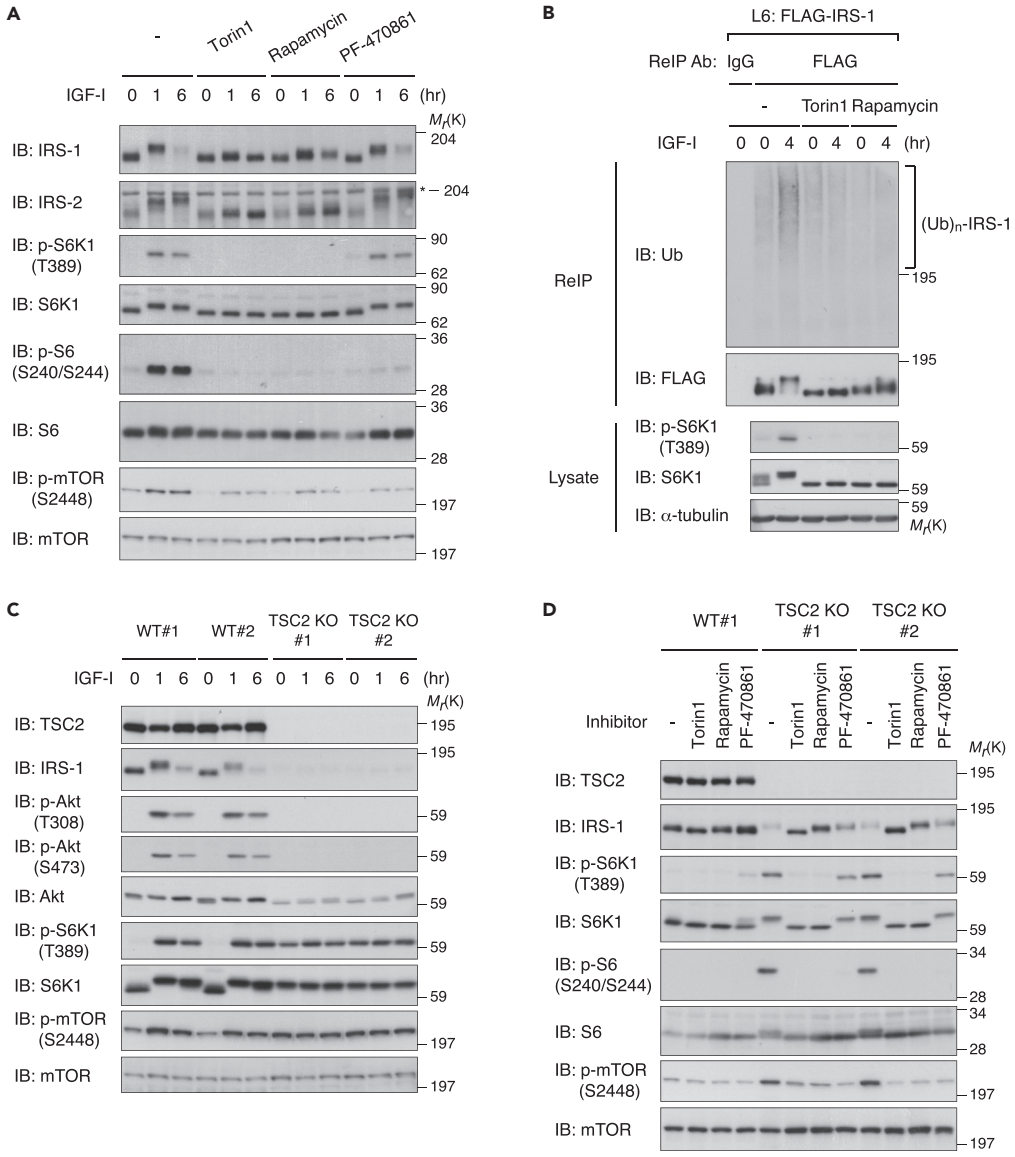

Figure 1. Activation of mTORC1 Is Necessary and Sufficient to Induce IRS-1 Degradation

(A) Immunoblot (IB) analysis of whole-cell lysates derived from L6 cells that were serum starved, treated with the indicated inhibitors, and then collected at the indicated time periods following IGF-I stimulation. Asterisk indicates a non-specific band.

(B) L6 cells stably expressing FLAG-IRS-1 (L6: FLAG-IRS-1) were serum starved and then collected at the indicated time periods following IGF-I stimulation. The cell lysates were subjected to immunoprecipitation (IP) with anti-FLAG antibody, and the bound proteins were eluted under denaturing conditions. The denatured fraction was then re-immunoprecipitated (ReIP) with the indicated antibody for ubiquitination assay as described in Transparent Methods. Samples were analyzed by immunoblotting with the indicated antibodies.

(C) L6 cells lacking TSC2 (TSC2 KO) and wild-type (WT) cells were serum starved and then collected at the indicated time periods following IGF-I stimulation. The cell lysates were subjected to immunoblotting with the indicated antibodies. See also Figure S1D.

(D) Immunoblot analysis of whole-cell lysates derived from L6 WT and TSC2 KO cells that were serum starved with the indicated inhibitors for 12 hr.

The data shown are representative of three independent experiments. See also Figure S1.

Cullin1 is a scaffold protein of the Skp1/Cullin1/F box protein (SCF) E3 ligase complex (Duda et al., 2011).The SCF complex contains, in addition to Cullin1, the RING-finger protein Rbx1, the adaptor protein Skp1, a specific E2 enzyme, and an F box protein that recognizes the specific substrates.

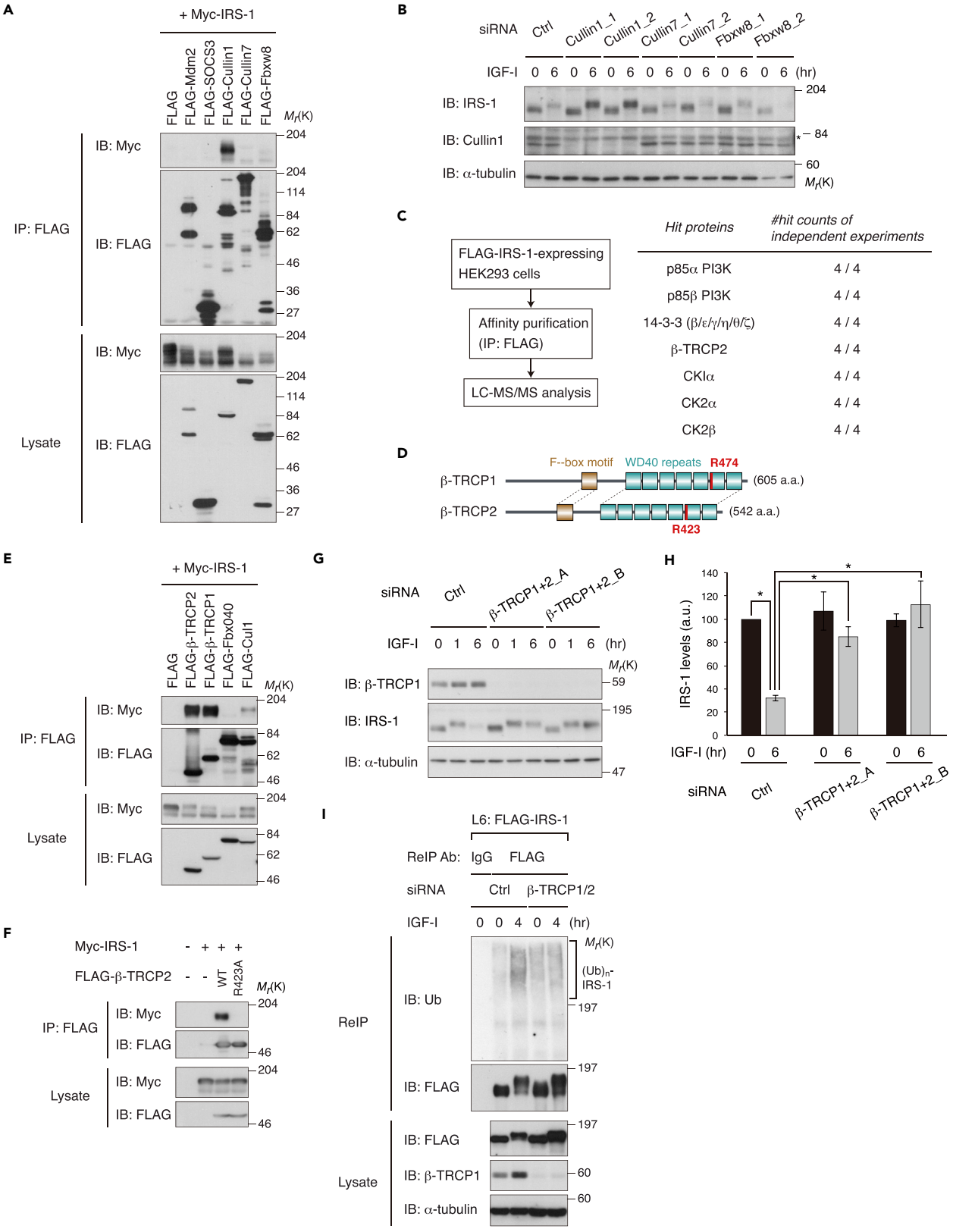
A
+ Myc-IRS-1
FLAG
FLAG-Mdm2
FLAG-SOCS3
FLAG-Cullin1
FLAG-Cullin7
FLAG-Fbxw8
Mr(K)
IP: FLAG
IB: Myc
IB: FLAG
Lysate
IB: Myc
IB: FLAG
204
114
84
62
46
36
27
B
siRNA
Ctrl
Cullin1_1
Cullin1_2
Cullin7_1
Cullin7_2
Fbxw8_1
Fbxw8_2
IGF-I 0 6 0 6 0 6 0 6 0 6 0 6 0 6 (hr)
IB: IRS-1
IB: Cullin1
IB: α-tubulin
204
84
60
Mr(K)
C
FLAG-IRS-1-expressing HEK293 cells
Affinity purification (IP: FLAG)
LC-MS/MS analysis
Hit proteins
#hit counts of independent experiments
p85α PI3K 4 / 4
p85β PI3K 4 / 4
14-3-3 (β/ε/γ/η/θ/ζ) 4 / 4
β-TRCP2 4 / 4
CKIα 4 / 4
CK2α 4 / 4
CK2β 4 / 4
D
F--box motif
WD40 repeats
R474
β-TRCP1
(605 a.a.)
β-TRCP2
(542 a.a.)
R423
E
+ Myc-IRS-1
FLAG
FLAG-β-TRCP2
FLAG-β-TRCP1
FLAG-Fbx040
FLAG-Cul1
Mr(K)
IP: FLAG
IB: Myc
IB: FLAG
Lysate
IB: Myc
IB: FLAG
204
84
62
46
F
Myc-IRS-1 - + + +
FLAG-β-TRCP2 - - WT R423A
Mr(K)
IP: FLAG
IB: Myc
IB: FLAG
Lysate
IB: Myc
IB: FLAG
204
46
G
siRNA
Ctrl
β-TRCP1+2_A
β-TRCP1+2_B
IGF-I 0 1 6 0 1 6 0 1 6 (hr)
Mr(K)
IB: β-TRCP1
IB: IRS-1
IB: α-tubulin
59
195
47
H
IRS-1 levels (a.u.)
140
120
100
80
60
40
20
0
IGF-I (hr) 0 6 0 6 0 6
siRNA
Ctrl
β-TRCP1+2_A
β-TRCP1+2_B
I
L6: FLAG-IRS-1
ReIP Ab: IgG FLAG
siRNA
Ctrl
β-TRCP1/2
IGF-I 0 0 4 0 4 (hr)
Mr(K)
ReIP
IB: Ub
(Ub)n-IRS-1
IB: FLAG
197
Lysate
IB: FLAG
IB: β-TRCP1
IB: α-tubulin
197
60
60

Figure 2. Cullin1 and β-TRCP1/2 Are Required for IRS-1 Degradation Induced by Prolonged IGF Stimulation

(A) HEK293T cells were transfected with Myc-IRS-1 together with the indicated E3 ligase components, and lysates were subjected to anti-FLAG immunoprecipitation (IP) and immunoblotting (IB) with the indicated antibodies.

(B) L6 cells were transfected with siRNA targeting the indicated E3 ligase components, serum starved, and then collected at the indicated time periods following IGF-I stimulation. Asterisk indicates a non-specific band. The knockdown efficiency of Cullin7 and Fbxw8 was validated by quantitative RT-PCR shown in Figure S2A.

(C) FLAG-IRS-1 was transiently expressed in HEK293 cells, and the protein complex of FLAG-IRS-1 was isolated with anti-FLAG immunoprecipitation and subjected to liquid chromatography-tandem mass spectrometry (LC-MS/MS) analysis. The recovered IRS-1-associated proteins and their reproducibility from four independent experiments are shown.

(D) Schematic structure of human β-TRCP1 and β-TRCP2. The substrate recognition site R474 in β-TRCP1 and its homologous site R423 in β-TRCP2 are depicted in red.

(E) HEK293T cells were transfected with Myc-IRS-1 together with the indicated F box proteins, and lysates were subjected to anti-FLAG immunoprecipitation and immunoblotting with the indicated antibodies.

(F) HEK293T cells were transfected with Myc-IRS-1 together with FLAG-β-TRCP2 WT or R423A mutant, and lysates were subjected to anti-FLAG immunoprecipitation and immunoblotting with the indicated antibodies.

(G and H) L6 cells were transfected with two siRNAs targeting β-TRCP1 and β-TRCP2, serum starved, and then collected at the indicated time periods following IGF-I stimulation. The cell lysates were subjected to immunoblotting with the indicated antibodies. The knockdown efficiency of β-TRCP2 was validated by quantitative RT-PCR shown in Figure S2D. Immunoblots of IRS-1 for (G) were quantified, and the graph is shown as mean ± SEM of three independent experiments (*$p < 0.05$) (H).

(I) L6 cells stably expressing FLAG-IRS-1 (L6: FLAG-IRS-1) were transfected with two siRNAs targeting β-TRCP1 and β-TRCP2, serum starved, and then collected at the indicated time periods following IGF-I stimulation. The cell lysates were subjected to re-immunoprecipitation (ReIP) with anti-FLAG antibody under denatured conditions for ubiquitination assay as described in Transparent Methods. Samples were analyzed by immunoblotting with the indicated antibodies.

The data shown are representative of at least three independent experiments. See also Figures S2 and S3.

Among numerous F box proteins, we identified β-TRCP2 (β-transducin repeat-containing protein 2) as an IRS-1-associated protein by mass spectrometry analysis of proteins co-purified with IRS-1 (Figure 2C). In mammals, a paralog designated as β-TRCP1 is also expressed, which has similar properties in the domain structure as β-TRCP2 (Figure 2D). Co-immunoprecipitation analysis revealed that both β-TRCP1 and β-TRCP2 bound to IRS-1, whereas the interaction of IRS-1 with Fbxo40, a skeletal muscle-specific F box protein of the SCF complex targeting IRS-1 for degradation (Shi et al., 2011), was hardly detected in 293T cells (Figure 2E). In addition, IRS-1 displayed a significantly reduced interaction with β-TRCP2 R423A harboring a point mutation within the substrate interaction site of β-TRCP2, which is homologous to R474A of β-TRCP1 (Wu et al., 2003) (Figures 2D and 2F). To determine whether IRS-1 is targeted by the $SCF^{\beta\text{-}TRCP1/2}$ complex for degradation, we assessed IRS-1 protein abundance in cells after depleting β-TRCP1/2. Although knockdown of β-TRCP1 or β-TRCP2 alone had minor effects on the IRS-1 abundance (Figures S2B–S2D), simultaneous knockdown of both β-TRCP1 and β-TRCP2 led to the inhibition of IRS-1 degradation induced by prolonged IGF-I stimulation (Figures 2G and 2H). Furthermore, IGF-I-induced polyubiquitination of IRS-1 was reduced in the β-TRCP (β-TRCP1 and β-TRCP2)-depleted cells (Figure 2I). Collectively, these data indicate that the $SCF^{\beta\text{-}TRCP}$ E3 ligase complex is required for IGF-I-dependent degradation of IRS-1.

IGF Stimulation Triggers the Interaction of IRS-1 with β-TRCP in an mTORC1-Dependent Manner

We next asked whether IRS-1 degradation induced by mTORC1 activation depends on the $SCF^{\beta\text{-}TRCP}$ complex. In L6 TSC2 KO cells in which the IRS-1 level is markedly suppressed, knockdown of β-TRCP or Cullin1 restored the IRS-1 levels under serum starvation conditions (Figure 3A), suggesting that constitutively elevated activation of mTORC1 leads to $SCF^{\beta\text{-}TRCP}$-mediated degradation of IRS-1. Accumulated evidence has demonstrated that phosphorylation of the degron motif (a specific sequence that directs the recognition of an E3 ligase) in substrates by specific kinase(s) is required for the substrate ubiquitination by the $SCF^{\beta\text{-}TRCP}$ complex (Frescas and Pagano, 2008; Wang et al., 2014). In agreement with this, IGF-I stimulated the interaction of IRS-1 with β-TRCP1, and treatment with Torin1 completely abolished it (Figure 3B). To a lesser extent, treatment with rapamycin blocked the IGF-I-induced increase in the IRS-1-β-TRCP1 interaction, whereas treatment with PF-470861 had minor effects on it (Figure 3B).

We noticed that IGF-I stimulation (1–3 hr) increased the expression of β-TRCP1 in L6 cells (Figures 2G and 2I). Rapamycin and PF-470861 had modest effects, whereas Torin1 significantly inhibited IGF-I-induced upregulation of β-TRCP1 protein levels (Figure S3A). Torin1 also reduced the IGF-I-stimulated increase in β-TRCP1 and β-TRCP2 mRNA levels (Figure S3B), indicating the role of mTOR in positively regulating β-TRCP expression.

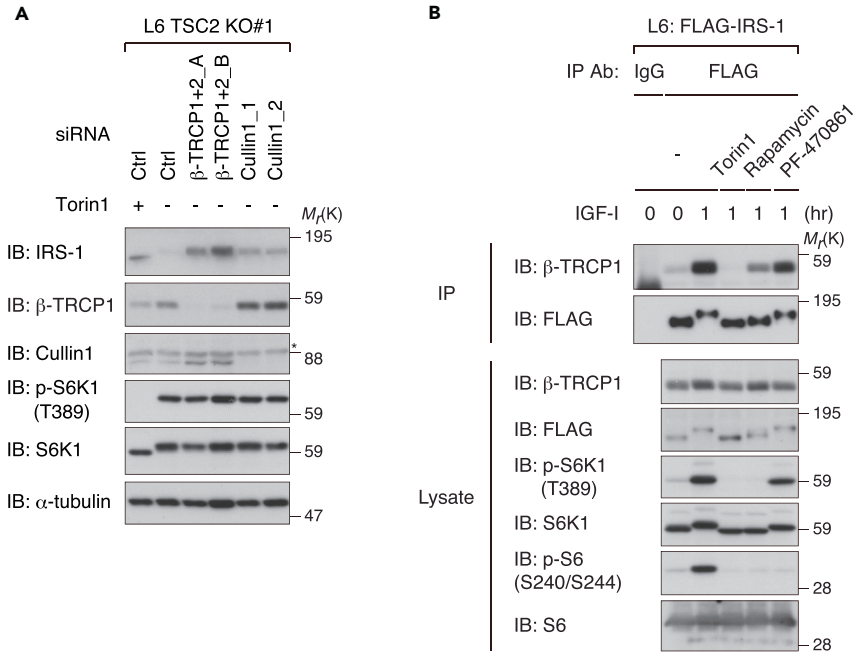

Figure 3. IGF Stimulation Triggers the Interaction of IRS-1 with β-TRCP in an mTORC1-Dependent Manner

(A) L6 TSC2 KO cells were transfected with siRNAs targeting β-TRCP1+2 or Cullin1 and serum starved with or without Torin1 for 12 hr. The collected cell lysates were subjected to immunoblotting (IB) with the indicated antibodies. Asterisk indicates a non-specific band.

(B) L6 cells stably expressing FLAG-IRS-1 (L6: FLAG-IRS-1) were serum starved, treated with the indicated inhibitors, and then collected at the indicated time periods following IGF-I stimulation. The cell lysates were subjected to immunoprecipitation (IP) and immunoblotting with the indicated antibodies.

The data shown are representative of three independent experiments. See also Figure S3.

Mapping of the Degron-Containing Region in IRS-1

We reasoned that if mTORC1 activation leads to the recruitment of β-TRCP to IRS-1 and subsequent IRS-1 degradation, the mutation of rapamycin/Torin1-responsive Ser/Thr residues in IRS-1 could block its degradation. Ser 302, Ser 307, and Ser 318 in IRS-1 were phosphorylated in an mTOR-dependent manner (Figure S1B). In addition, Ser 522 has been reportedly required for IRS-1 degradation (Xu et al., 2008). However, single mutation of these Ser residues or mutation of all of them could not block IRS-1 degradation induced by prolonged IGF-I stimulation (Figures S4A and S4B), indicating that the known Ser residues of IRS-1 are not necessary for mTORC1-dependent degradation of IRS-1.

We then mapped the corresponding region of IRS-1 involved in its degradation. Using a series of IRS-1 deletion mutants, we examined the abundance of these IRS-1 mutants after prolonged IGF-I stimulation (Figure S4C). Since some IRS-1 mutants exhibited large mobility upshift in SDS-PAGE, we treated the cell lysates with alkaline phosphatase to place them in comparable electrophoretic mobility. The IRS-1 mutants encompassing amino acid residues 1–1,000, 1–600, and 301–1,235, and the full-length (1–1,235) exhibited the degradation 6 hr after IGF-I stimulation, whereas the mutants encompassing amino acid residues 1–500, 1–300, 501–1,235, and 601–1,235 were resistant to the IGF-I-induced degradation (Figure S4D). These data suggest that the region corresponding to amino acid residues 301–500 or 501–600 in IRS-1 is required for its degradation induced by prolonged IGF-I stimulation.

To examine whether Ser/Thr residues in the IRS-1 region corresponding to amino acid residues 301–600 are required for IRS-1 degradation, we first selected putative 48 Ser/Thr residues that are authenticated phosphosites largely based on reported mass spectrometry analyses according to the PhosphoSite program (Hornbeck et al., 2015) (Figure S4E). We then constructed the IRS-1 mutant in which all 48 Ser/Thr residues are substituted with Ala residues (IRS-1 STA 301–600) (Figure 4A). The IRS-1 STA 301–600 mutant was not degraded after prolonged IGF-I stimulation (Figure 4B). We further analyzed two IRS-1 mutants in which the mutation in IRS-1 STA 301–600 was introduced into the region corresponding to amino acid residues

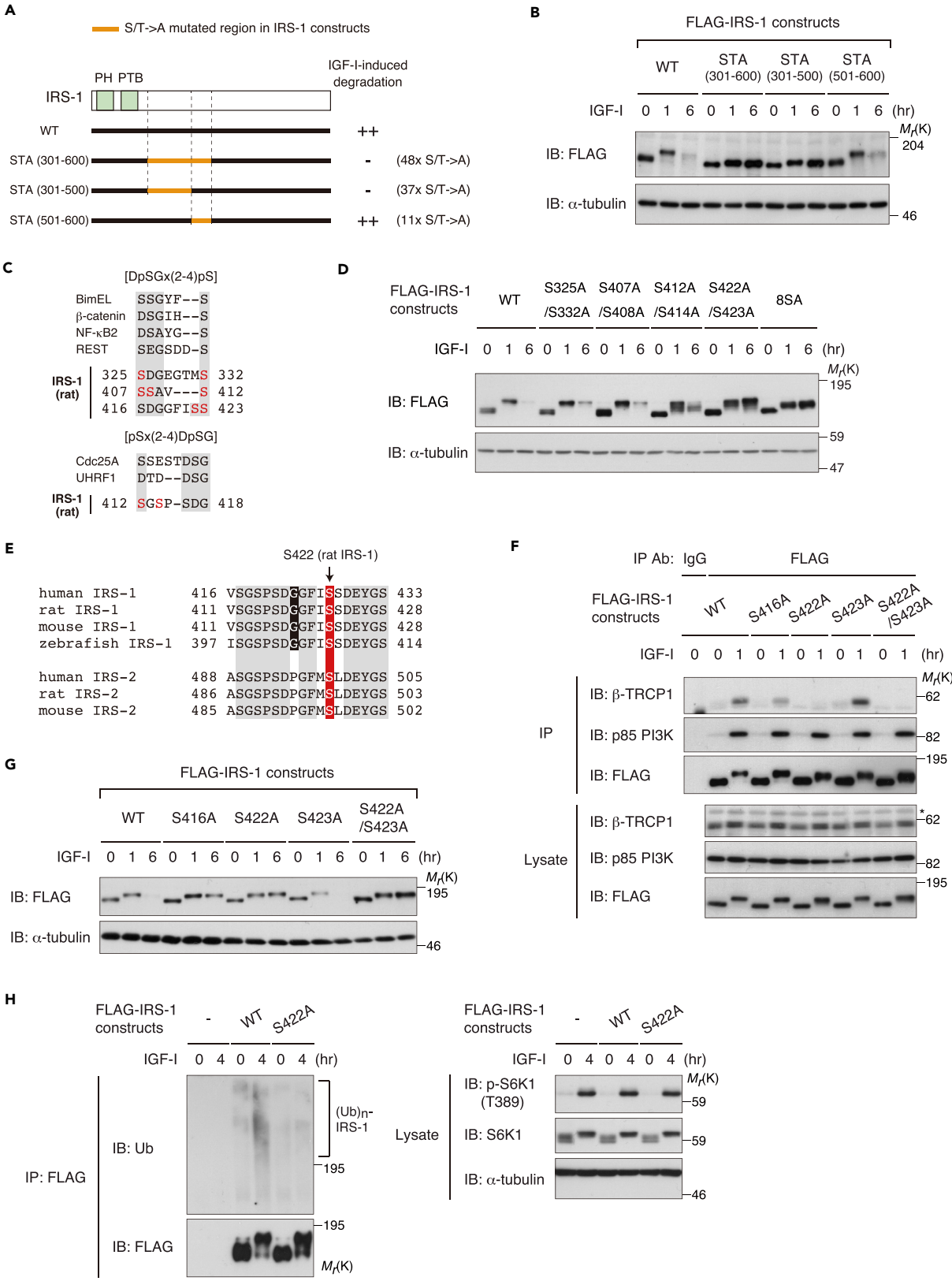
A
S/T->A mutated region in IRS-1 constructs
PH PTB
IRS-1
IGF-I-induced degradation
WT ++
STA (301-600) - (48x S/T->A)
STA (301-500) - (37x S/T->A)
STA (501-600) ++ (11x S/T->A)
B
FLAG-IRS-1 constructs
WT
STA (301-600)
STA (301-500)
STA (501-600)
IGF-I 0 1 6 0 1 6 0 1 6 0 1 6 (hr)
IB: FLAG
IB: α-tubulin
Mr(K)
204
46
C
[DpSGx(2-4)pS]
BimEL SSGYF--S
β-catenin DSGIH--S
NF-κB2 DSAYG--S
REST SEGSDD-S
IRS-1 (rat)
325 SDGEGTMS 332
407 SSAV---S 412
416 SDGGFISS 423
[pSx(2-4)DpSG]
Cdc25A SSESTDSG
UHRF1 DTD--DSG
IRS-1 (rat)
412 SGSP-SDG 418
D
FLAG-IRS-1 constructs
WT
S325A /S332A
S407A /S408A
S412A /S414A
S422A /S423A
8SA
IGF-I 0 1 6 0 1 6 0 1 6 0 1 6 0 1 6 0 1 6 (hr)
IB: FLAG
IB: α-tubulin
Mr(K)
195
59
47
E
S422 (rat IRS-1)
human IRS-1 416 VSGSPSDGGFISSDEYGS 433
rat IRS-1 411 VSGSPSDGGFISSDEYGS 428
mouse IRS-1 411 VSGSPSDGGFISSDEYGS 428
zebrafish IRS-1 397 ISGSPSDGGFISSDEYGS 414
human IRS-2 488 ASGSPSDPGFMSLDEYGS 505
rat IRS-2 486 ASGSPSDPGFMSLDEYGS 503
mouse IRS-2 485 ASGSPSDPGFMSLDEYGS 502
F
IP Ab: IgG FLAG
FLAG-IRS-1 constructs
WT
S416A
S422A
S423A
S422A /S423A
IGF-I 0 0 1 0 1 0 1 0 1 0 1 (hr)
IP
IB: β-TRCP1
IB: p85 PI3K
IB: FLAG
Lysate
IB: β-TRCP1
IB: p85 PI3K
IB: FLAG
Mr(K)
62
82
195
*
G
FLAG-IRS-1 constructs
WT
S416A
S422A
S423A
S422A /S423A
IGF-I 0 1 6 0 1 6 0 1 6 0 1 6 0 1 6 (hr)
IB: FLAG
IB: α-tubulin
Mr(K)
195
46
H
FLAG-IRS-1 constructs
-
WT
S422A
IGF-I 0 4 0 4 0 4 (hr)
IP: FLAG
IB: Ub
(Ub)n-IRS-1
195
IB: FLAG
195
Mr(K)
Lysate
IB: p-S6K1 (T389)
IB: S6K1
IB: α-tubulin
Mr(K)
59
59
46

Figure 4. Ser 422 in IRS-1 Is Required for the Interaction with β-TRCP and IGF-I-Induced Degradation of IRS-1

(A) Schematic illustration of IRS-1 mutants used in (B). The regions colored in orange include the Ala substitution of possible phosphorylated Ser/Thr residues that are authenticated in PhosphoSitePlus. See also Figure S4E.

(B) Immunoblot (IB) analysis of whole-cell lysates derived from L6 cells stably expressing the indicated FLAG-IRS-1 mutants that were serum starved and then collected at the indicated time periods following IGF-I stimulation.

(C) Schematic representation of the candidate β-TRCP recognition sites that are included in the IRS-1 region corresponding to amino acid residues 301–501. The Ser residues colored in red indicate the authenticated phosphosites that are listed in PhosphoSitePlus.

(D) Immunoblot analysis of whole-cell lysates derived from L6 cells stably expressing the indicated FLAG-IRS-1 mutants that were serum starved and then collected at the indicated time periods following IGF-I stimulation.

(E) Amino acid sequence alignment of Ser 422 and its surrounding sequence among IRS-1 proteins of vertebrates. Identical residues are highlighted in gray, a critical Ser for IRS-1 degradation is in red, and Gly, a conserved residue only in IRS-1 but not in IRS-2, is in black.

(F) L6 cells stably expressing the indicated FLAG-IRS-1 mutants were serum starved and then collected at the indicated time periods following IGF-I stimulation. The cell lysates were subjected to immunoprecipitation (IP) and immunoblotting with the indicated antibodies.

(G) Immunoblot analysis of whole-cell lysates derived from L6 cells stably expressing the indicated FLAG-IRS-1 mutants that were serum starved and then collected at the indicated time periods following IGF-I stimulation.

(H) L6 cells stably expressing FLAG-IRS-1 WT, S422A, or empty vector were serum starved and then collected at the indicated time periods following IGF-I stimulation. The cell lysates were subjected to re-immunoprecipitation (ReIP) with anti-FLAG antibody under denatured conditions for ubiquitination assay as described in Transparent Methods. Samples were analyzed by immunoblotting with the indicated antibodies.

The data shown are representative of three independent experiments. See also Figure S4.

301–500 and 501–600. Although the IRS-1 STA 501–600 level was significantly reduced after prolonged IGF-I stimulation, IRS-1 STA 301–500 failed to undergo IGF-I-stimulated degradation (Figure 4B), revealing the existence of responsible Ser/Thr residues in the IRS-1 301–500 region for the degradation induced by prolonged IGF-I stimulation.

Ser 422 in IRS-1 Is Required for the Interaction with β-TRCP and IGF-I-Induced Degradation of IRS-1

The canonical degron recognized by β-TRCP contains the DpSGx(2-4)pS in which Ser residues are phosphorylated (Frescas and Pagano, 2008). In addition, the pSx(2-4)DpSG degron has been demonstrated to be recognized by β-TRCP. These phospho-degrons can diverge from the canonical motifs, with phospho-Ser replacing the acidic residues. The region of IRS-1 responsible for its degradation (amino acid residues 301–500) contains S^{325}DGEGTMS^{332}, S^{407}SAVS^{412}, S^{412}GSPSDG^{418}, and S^{416}DGGFISS^{423} (Figure 4C). Among these sequences, we mutated the Ser residues, which are authenticated phosphorylation sites in the PhosphoSite program, into Ala (we mutated each Ser residue into Ala in S325A/S332A, S407A/S408A, S412A/S414A, and S422A/S423A, and all eight Ser residues were replaced with Ala in 8SA) and examined IRS-1 levels after IGF-I stimulation. The IRS-1 S422A/S423A mutant, as well as the 8SA mutant, failed to undergo the degradation induced by prolonged IGF-I stimulation (Figure 4D). The S^{416}DGGFISS^{423} sequence in IRS-1 is highly conserved among vertebrates, whereas they differ from the identical site in IRS-2, including the third residue substitution from Gly to Pro (Figure 4E).

We next determined the critical Ser residue(s) of IRS-1 for β-TRCP recognition of IRS-1 among the S^{416}DGGFISS^{423} sequence. The IRS-1 mutant S422A, but not S423A, failed to interact with β-TRCP1 in response to IGF-I stimulation (Figure 4F). The IRS-1 S416A mutant showed partial reduction in the interaction with β-TRCP1, although the phosphorylation of IRS-1 Ser 416 has not been reported (Figure 4F). In addition, the IRS-1 S416A, S422A, and S422A/S423A mutants failed to undergo IGF-I-stimulated degradation, whereas the IRS-1 S423A showed similar degradation as the wild-type IRS-1 (Figure 4G). Finally, the IRS-1 S422A mutant failed to undergo IGF-I-stimulated polyubiquitination as revealed by ubiquitination assay (Figure 4H). These results clearly demonstrate that the Ser 422 in IRS-1 is essential for the interaction with β-TRCP and IGF-I-induced degradation of IRS-1.

mTORC1 Phosphorylates Ser 422 of IRS-1 in IGF-Stimulated Cells

We set out to find out how Ser 422 phosphorylation of IRS-1 is regulated. To generate phospho-IRS-1-specific antibody, we chose the S^{416}DGGFI(pS^{422})(pS^{423}) phospho-peptide as an antigen since the dual phosphorylated, but neither individually phosphorylated, peptide has been identified by the previous phosphoproteomic study (Humphrey et al., 2013). We confirmed that this antibody selectively recognized phosphorylated IRS-1 but not the S422A/S423A mutant of IRS-1 nor dephosphorylated IRS-1 treated with alkaline phosphatase *in vitro* (Figure 5A). The phospho-IRS-1 (S422/S423) antibody detected significantly less of the S422A or S423 mutant of IRS-1 than wild-type IRS-1, suggesting that this antibody recognizes dual phosphorylation of Ser 422 and Ser 423 (Figure 5A). As expected, IGF-I stimulation increased IRS-1

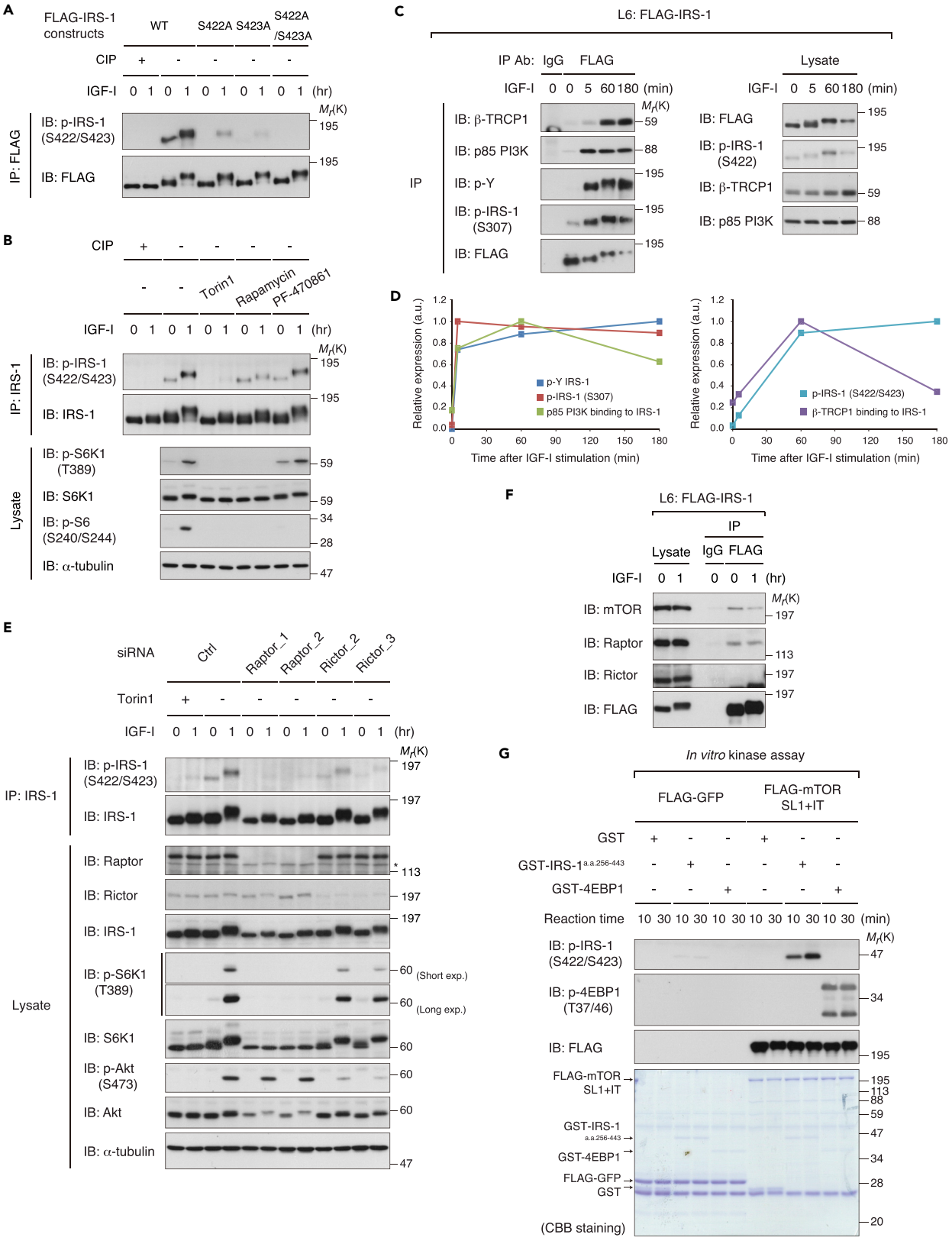
A
FLAG-IRS-1 constructs
WT
S422A
S423A
S422A /S423A
CIP
IGF-I
(hr)
IP: FLAG
IB: p-IRS-1 (S422/S423)
IB: FLAG
M_r(K)
B
Torin1
Rapamycin
PF-470861
IP: IRS-1
IB: IRS-1
Lysate
IB: p-S6K1 (T389)
IB: S6K1
IB: p-S6 (S240/S244)
IB: α-tubulin
C
L6: FLAG-IRS-1
IP Ab: IgG FLAG
Lysate
(min)
IP
IB: β-TRCP1
IB: p85 PI3K
IB: p-Y
IB: p-IRS-1 (S307)
IB: FLAG
IB: p-IRS-1 (S422)
D
Relative expression (a.u.)
p-Y IRS-1
p-IRS-1 (S307)
p85 PI3K binding to IRS-1
p-IRS-1 (S422/S423)
β-TRCP1 binding to IRS-1
Time after IGF-I stimulation (min)
E
siRNA
Ctrl
Raptor_1
Raptor_2
Rictor_2
Rictor_3
IB: Raptor
IB: Rictor
(Short exp.)
(Long exp.)
IB: Akt
IB: p-Akt (S473)
F
L6: FLAG-IRS-1
IP
Lysate
IgG FLAG
IB: mTOR
G
In vitro kinase assay
FLAG-GFP
FLAG-mTOR SL1+IT
GST
GST-IRS-1 a.a.256-443
GST-4EBP1
Reaction time
(min)
IB: p-4EBP1 (T37/46)
FLAG-mTOR SL1+IT
GST-IRS-1 a.a.256-443
FLAG-GFP
GST
(CBB staining)

Figure 5. mTORC1 Phosphorylates Ser 422 of IRS-1 in IGF-Stimulated Cells

(A) p-IRS-1 (S422/S423) antibody preferentially recognizes S422/S423-phosphorylated IRS-1. L6 cells stably expressing the indicated FLAG-IRS-1 mutants were serum starved and then collected at the indicated time periods following IGF-I stimulation. FLAG-IRS-1 was immunoprecipitated (IP), and one set of the WT immunoprecipitates was treated with calf intestine alkaline phosphatase (CIP). The immunoprecipitated IRS-1 phosphorylation and protein levels were then detected by immunoblotting (IB) with anti-p-IRS-1 (S422/S423) antibody and anti-FLAG antibody, respectively.

(B) L6 cells were serum starved, treated with the indicated inhibitors, and then collected at the indicated time periods following IGF-I stimulation. The endogenous IRS-1 proteins were immunoprecipitated, and one set of the immunoprecipitates was treated with CIP. The immunoprecipitated IRS-1 phosphorylation and S6K1/S6 phosphorylation were analyzed by immunoblotting with the indicated antibodies.

(C and D) L6 cells stably expressing FLAG-IRS-1 (L6: FLAG-IRS-1) were serum starved and then collected at the indicated time periods following IGF-I stimulation. The cell lysates were subjected to immunoprecipitation and immunoblotting with the indicated antibodies (C). Immunoblots of Tyr, Ser 307, and Ser 422/Ser 423 phosphorylation of IRS-1, and p85 PI3K and β-TRCP1 binding to IRS-1 for (C) were quantified and their time-dependent changes are shown in the graph (D).

(E) L6 cells were transfected with siRNA targeting Raptor or Rictor, serum starved, treated with or without Torin1, and then collected at the indicated time periods following IGF-I stimulation. The cell lysates were subjected to immunoprecipitation and immunoblotting with the indicated antibodies.

(F) L6 cells stably expressing FLAG-IRS-1 were serum starved and then collected at the indicated time periods following IGF-I stimulation. The cell lysates were subjected to immunoprecipitation and immunoblotting with the indicated antibodies against mTOR complex components. See also Figures S5E and S5F.

(G) *In vitro* phosphorylation of IRS-1 S422/S423 by mTOR. An active mutant FLAG-mTOR^{SL1+IT} and FLAG-GFP were expressed in HEK293T cells and were immunoprecipitated with anti-FLAG antibody. The substrates GST-IRS-1 fragment (amino acid residues 256–443), GST-4EBP1, and GST were expressed and purified from *Escherichia coli*. The kinase reaction was carried out as described in Transparent Methods. The phosphorylation levels of IRS-1 and 4EBP1 were analyzed by immunoblotting with anti-p-IRS-1 (S422/S423) antibody and p-4EBP1 (T37/46) antibody, respectively. The total amounts of recombinant proteins used were examined by Coomassie Brilliant Blue (CBB) staining. See also Figure S5G.

The data shown are representative of three independent experiments except Figures 5D and 5E being from two independent experiments. See also Figure S5.

Ser 422/Ser 423 phosphorylation in L6 cells (Figures 5A and 5B). Torin1 treatment completely abolished their phosphorylation of endogenous IRS-1, and rapamycin blocked their IGF-I-dependent increase, whereas PF-470861 did not significantly affect them (Figure 5B). The IGF-I-induced increase in Ser 422/Ser 423 phosphorylation of IRS-1 was also found to be sensitive to Torin1 and rapamycin in MEFs and primary mouse myoblasts (Figures S5A–S5C). Time course analyses revealed that IRS-1 Ser 422/Ser 423 phosphorylation was induced at a later period of IGF-I stimulation compared with Tyr and Ser 307 phosphorylation of IRS-1 and that the IRS-1 binding to β-TRCP1 followed the change in IRS-1 Ser 422/Ser 423 phosphorylation (Figures 5C and 5D).

We next sought to determine whether mTOR requires Raptor, an obligatory mTORC1 component, to phosphorylate IRS-1. In L6 cells, siRNA-mediated knockdown of Raptor significantly reduced basal and IGF-I-induced Ser 422/Ser 423 phosphorylation of IRS-1 (Figure 5E), indicating that mTORC1 is required for Ser 422/Ser 423 phosphorylation of IRS-1. In addition to IGF-I, amino acids are potent activators for mTORC1. In line with this, deprivation of amino acids diminished the basal phosphorylation of IRS-1 Ser 422/Ser 423, and amino acid stimulation, albeit to a lesser degree than IGF-I, induced phosphorylation of IRS-1 Ser 422/Ser 423 (Figure S5D). We also examined the contribution of mTORC2 to the IRS-1 phosphorylation by knocking down Rictor, an mTORC2-specific component. Although the Ser 422/Ser 423 phosphorylation of IRS-1 was modestly reduced in Rictor-depleted cells, mTORC1 activity monitored by Thr 389 phosphorylation of S6K1 was partly reduced probably due to impaired Akt activity in this context (Figure 5E), implying the possible role of mTORC2 in directly or indirectly phosphorylating IRS-1.

To gain further insight into mTORC1-dependent phosphorylation of IRS-1 Ser 422/Ser 423, we next examined the interaction of IRS-1 with mTORC1. Co-immunoprecipitation analysis revealed that mTOR and Raptor, but not Rictor, bound to IRS-1 (Figure 5F). We also found that FLAG-tagged Raptor bound to IRS-1 in HEK293T cells (Figure S5E). Using IRS-1 truncated mutants we mapped the region following the PTB domain (amino acid residues 260–542), which is necessary for the co-immunoprecipitation with mTOR and Raptor (Figure S5F). This region contains the SAIN (Shc and IRS-1 NPXY binding) domain, which has reportedly mediated the mTORC1 binding to IRS-1 (Tzatsos, 2009). Since Raptor is a scaffold that recruits downstream substrates to mTORC1 (Kim et al., 2002), we hypothesized that mTORC1 could directly phosphorylate Ser 422 of IRS-1. We purified GST-fused IRS-1$^{a.a.256–443}$ from *Escherichia coli* and mTOR complex containing an active mTOR mutant (mTOR^{SL1+IT}) from HEK293T cells (Ohne et al., 2008) and then subjected them to *in vitro* kinase assay (Figure S5G). Phosphorylation of Ser 422/Ser 423 in IRS-1 as well as a known mTORC1 substrate 4EBP1 was remarkably enhanced when incubated with the mTOR immunoprecipitates (Figure 5G). These data indicate that mTORC1 phosphorylates Ser 422 of IRS-1 in IGF-stimulated cells.

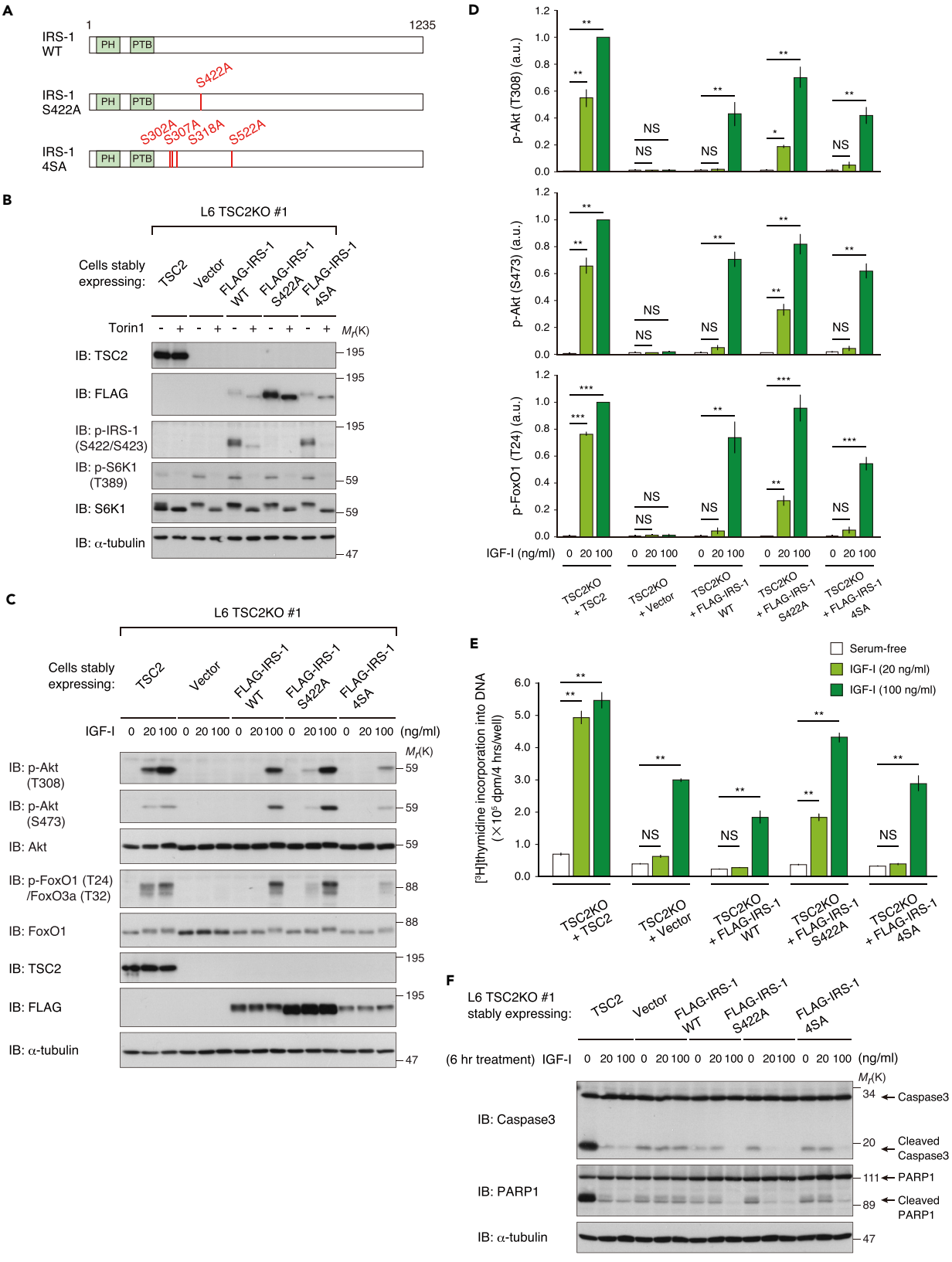
A
IRS-1 WT
IRS-1 S422A
IRS-1 4SA
PH
PTB
S422A
S302A
S307A
S318A
S522A
1
1235
B
L6 TSC2KO #1
Cells stably expressing:
TSC2
Vector
FLAG-IRS-1 WT
FLAG-IRS-1 S422A
FLAG-IRS-1 4SA
Torin1
IB: TSC2
IB: FLAG
IB: p-IRS-1 (S422/S423)
IB: p-S6K1 (T389)
IB: S6K1
IB: α-tubulin
C
IGF-I (ng/ml)
IB: p-Akt (T308)
IB: p-Akt (S473)
IB: Akt
IB: p-FoxO1 (T24) /FoxO3a (T32)
IB: FoxO1
D
p-Akt (T308) (a.u.)
p-Akt (S473) (a.u.)
p-FoxO1 (T24) (a.u.)
NS
TSC2KO + TSC2
TSC2KO + Vector
TSC2KO + FLAG-IRS-1 WT
TSC2KO + FLAG-IRS-1 S422A
TSC2KO + FLAG-IRS-1 4SA
E
Serum-free
IGF-I (20 ng/ml)
IGF-I (100 ng/ml)
[3H]thymidine incorporation into DNA (×10³ dpm/4 hrs/well)
F
L6 TSC2KO #1 stably expressing:
(6 hr treatment) IGF-I
IB: Caspase3
Caspase3
Cleaved Caspase3
IB: PARP1
PARP1
Cleaved PARP1

Figure 6. Expression of IRS-1 S422A Mutant Restores IGF-I Sensitivity in Cells Lacking TSC2

(A) Schematic illustration of wild-type (WT) IRS-1, IRS-1 S422A, and 4SA mutants.

(B) Immunoblot (IB) analysis of whole-cell lysates derived from L6 TSC2 KO cells stably expressing TSC2, FLAG-IRS-1 WT, S422A, 4SA, or empty vector that were serum starved and then collected at 1 hr following Torin1 stimulation.

(C and D) Immunoblot analysis of whole-cell lysates derived from L6 TSC2 KO cells stably expressing TSC2, FLAG-IRS-1 WT, S422A, 4SA, or empty vector that were serum starved and then collected at 5 min following IGF-I stimulation at the indicated concentration (C). Immunoblots of Akt and FoxO1/3a phosphorylation for (C) were quantified, and the graph is shown as mean ± SEM of four independent experiments (*$p < 0.05$, **$p < 0.01$, ***$p < 0.001$) (D).

(E) Effects of expression of TSC2 or IRS-1 mutants on IGF-I-induced DNA synthesis in L6 TSC2 KO cells. L6 TSC2 KO cells stably expressing TSC2, FLAG-IRS-1 WT, S422A, 4SA, or empty vector were serum starved and then treated with IGF-I at the indicated concentration for 12 hr. [^{3}H]Thymidine incorporation into DNA during 8–12 hr of IGF-I stimulation was measured. The graph is shown as mean ± SEM (n = 4; **$p < 0.01$).

(F) L6 TSC2 KO cells stably expressing TSC2, FLAG-IRS-1 WT, S422A, 4SA, or empty vector were placed in serum-free medium with or without IGF-I at the indicated concentration for 6 hr. The collected cell lysates were subjected to immunoblotting with the indicated antibodies. See also Figure S6A.

The data shown are representative of at least three independent experiments. See also Figure S6.

Expression of IRS-1 S422A Mutant Restores IGF-I Sensitivity in Cells Lacking TSC2

We next assessed whether Ser 422 phosphorylation-dependent degradation of IRS-1 causes insulin/IGF resistance in TSC2-deficient cells. To test this idea, we generated L6 TSC2 KO cells stably expressing IRS-1 S422A as well as IRS-1 WT (Figure 6A). Expression of IRS-1 S422A was significantly higher than that of IRS-1 WT in these cells under basal conditions (Figure 6B), which reflected their abilities to undergo mTORC1-dependent degradation. TSC2 KO cells expressing empty vector failed to phosphorylate Akt and its direct substrate FoxO1/3a in response to high-dose IGF-I (100 ng/mL), whereas rescue with TSC2 restored the sensitivity (Figure 6C). In the TSC2 KO cells expressing IRS-1 WT, phosphorylation of Akt and FoxO1/3a was not induced by low-dose IGF-I (20 ng/mL) (Figure 6C). Importantly, the TSC2 KO cells expressing IRS-1 S422A mutant could in part respond to low-dose IGF-I to phosphorylate Akt and FoxO1/3a (Figures 6C and 6D). We also compared the Akt signaling in the TSC2 KO cells expressing the IRS-1 4SA mutant, in which Ser 302, Ser 307, Ser 318, and Ser 522, which were phosphosites sensitive to mTOR inhibitors but were dispensable for degradation, are mutated to Ala (Figure 6A). The expression level of IRS-1 4SA was significantly lower than that of IRS-1 S422A in the TSC2 KO cells (Figure 6B). In addition, the TSC2 KO cells expressing IRS-1 4SA failed to respond to low-dose IGF-I for phosphorylation of Akt and FoxO1/3a to an extent similar to IRS-1 WT-expressing cells (Figures 6C and 6D), indicating that phosphorylation of Ser 422, but not other mTORC1 target sites, is responsible for mTORC1-mediated inhibition of Akt signaling in the TSC2-deficient state.

Since Akt signaling supports IGF-I-mediated cell proliferation and cell survival, we analyzed the growth and survival responses to IGF-I in L6 TSC2 KO cells expressing IRS-1 mutants. By measuring IGF-I-stimulated DNA synthesis, we found that TSC2 KO cells expressing IRS-1 S422A as well as TSC2-rescued cells showed growth response to low-dose IGF-I, whereas TSC2 KO cells expressing IRS-1 WT and 4SA as well as expressing empty vector only could not (Figure 6E).

The anti-apoptotic program induced by IGF-I is severely compromised in the TSC2-deficient state (Shah et al., 2004). We confirmed that IGF-I could not inhibit serum-starvation-induced cleavage of Caspase3 and its substrate PARP1 in L6 TSC2 KO cells and that rescue with TSC2 in these cells restored the anti-apoptotic effect of IGF-I (Figure 6F). We also observed that low-dose IGF-I inhibited cleavage of Caspase3 and PARP1 in TSC2 KO cells expressing IRS-1 S422A but not IRS-1 WT nor 4SA (Figure 6F). Similar trends in IGF-I-mediated cell survival response were observed by analyzing Annexin V-positive apoptotic cells using flow cytometry (Figure S5A). These data collectively indicate that expression of IRS-1 S422A, but not of IRS-1 WT or 4SA, effectively restores the growth and survival responses to IGF through Akt activation in the TSC2-deficient state (Figure S6B).

Inhibition of Ser 422 Phosphorylation-Dependent IRS-1 Degradation Promotes Sustained Akt Activation in IGF-Stimulated Cells

Previous studies have demonstrated that long-term IGF/insulin stimulation induces IRS-1 degradation with a concomitant decrease in Akt activity in various types of cells (Haruta et al., 2000; Kim et al., 2012; Shi et al., 2011; Yoneyama et al., 2018). To investigate how mTORC1- and SCF$^{\beta\text{-TRCP}}$-mediated degradation of IRS-1 influences IGF signaling, we knocked down β-TRCP in L6 cells to inhibit IGF-I-stimulated degradation of IRS-1. Although phosphorylation of Akt was gradually decreased upon prolonged IGF-I stimulation in control cells, loss of β-TRCP resulted in sustained Akt phosphorylation (Figures 7A and 7B). We also found that expression of IRS-1 S422A, but not of IRS-1 WT, promoted sustained Akt phosphorylation up to 12 hr

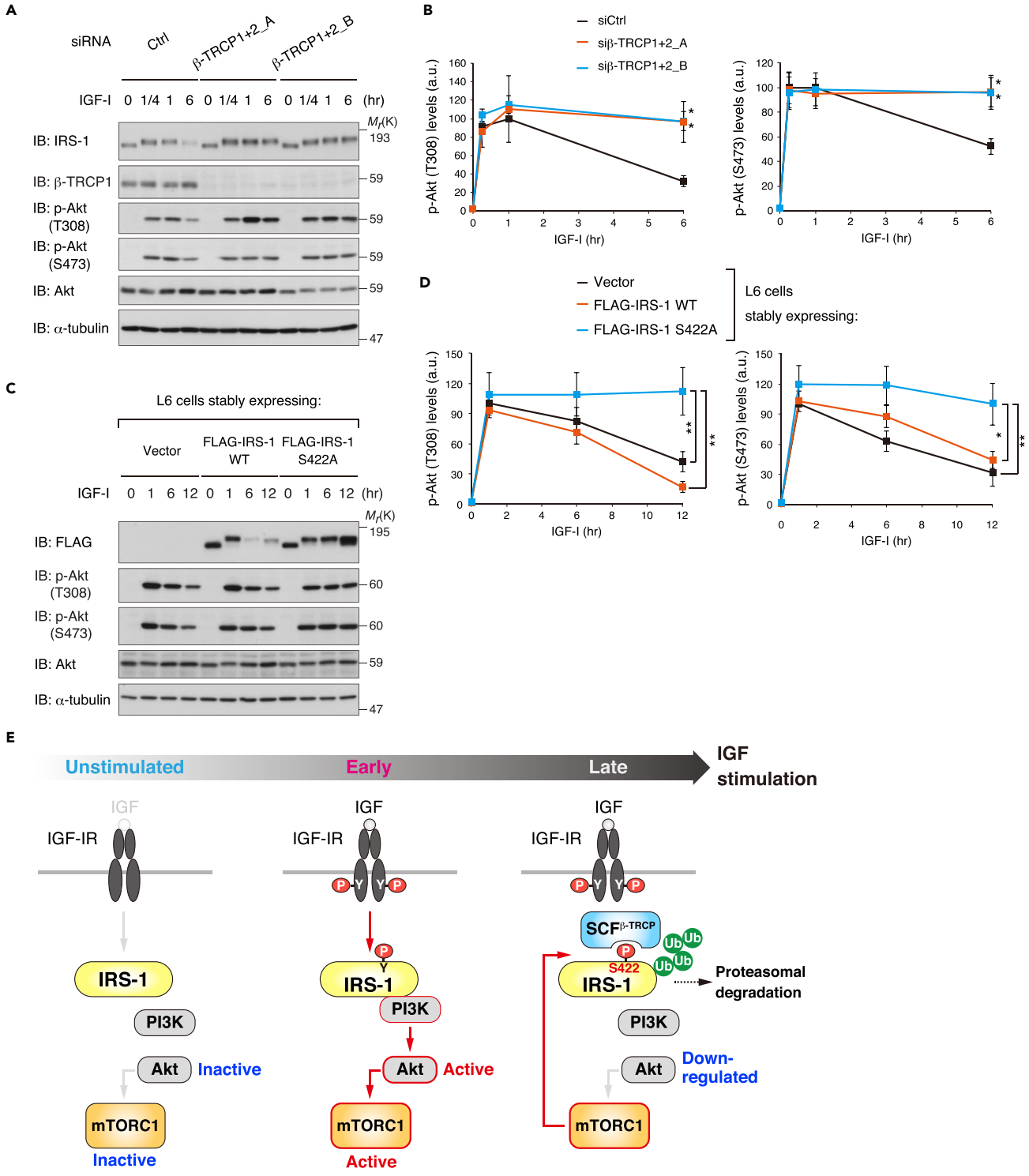

Figure 7. Inhibition of Ser 422 Phosphorylation-Dependent IRS-1 Degradation Promotes Sustained Akt Activation in IGF-Stimulated Cells

(A and B) L6 cells were transfected with two siRNAs targeting β-TRCP1 and β-TRCP2, serum starved, and then collected at the indicated time periods following IGF-I stimulation. The cell lysates were subjected to immunoblotting (IB) with the indicated antibodies (A). Immunoblots of Akt phosphorylation for (A) were quantified, and the graph is shown as mean ± SEM of four independent experiments (*$p < 0.05$) (B).

Figure 7. *Continued*

(C and D) Immunoblot analysis of whole-cell lysates derived from L6 cells stably expressing FLAG-IRS-1 WT, S422A, or empty vector that were serum starved and then collected at the indicated time periods following IGF-I stimulation (C). Immunoblots of Akt phosphorylation for (C) were quantified, and the graph is shown as mean ± SEM of three independent experiments (*$p < 0.05$, **$p < 0.01$) (D).

(E) Model for temporal regulation of mTORC1-mediated IRS-1 degradation and the PI3K/Akt signaling following IGF stimulation. The figure depicts the interplay of mTORC1-induced Ser 422 phosphorylation of IRS-1, $SCF^{\beta\text{-}TRCP}$-mediated ubiquitination of IRS-1, and downregulation of the PI3K/Akt signaling as a function of time following the stimulation. See text for details.

stimulation of IGF-I in L6 cells (Figures 7C and 7D). These data indicate that inhibition of IRS-1 degradation can enhance sustained activation of Akt in response to IGF.

DISCUSSION

IRS-1 function is regulated through complex mechanisms involving phosphorylation of at least 70 Ser/Thr residues within its C-terminal tail region (Copps and White, 2012). Since insulin/IGF-stimulated downstream kinases phosphorylate Ser/Thr residues in IRS-1, the autologous Ser/Thr phosphorylation of IRS-1 is in general regarded as a feedback loop to tightly regulate the strength or duration of the insulin/IGF signaling (Harrington et al., 2005). The data we presented in this study reveal that Ser 422 of IRS-1, which has no previously characterized regulatory role, is critical for mTORC1-mediated degradation of IRS-1. The mechanism is as follows. IGF stimulates mTORC1, which then phosphorylates Ser 422 of IRS-1. Phosphorylation of Ser 422 creates the binding site of the $SCF^{\beta\text{-}TRCP}$ E3 ligase in IRS-1, leading to subsequent ubiquitination and degradation of IRS-1. Our study reveals that mTORC1-mediated degradation of IRS-1 is a regulatory node determining the duration of IGF signaling (Figure 7E).

Multiple lines of evidence support the conclusion that Ser 422 is a *bona fide* target phosphorylation site of mTORC1. First, Torin1 and rapamycin inhibited IGF-I-induced phosphorylation of IRS-1 Ser 422 (Figure 5B). Second, knockdown of Raptor resulted in the loss of this phosphorylation under both basal and IGF-I-stimulated conditions, which was also caused by Torin1 (Figure 5E). Third, serum and amino acid starvation reduced the basal phosphorylation of IRS-1 Ser 422, and the add-back of amino acids increased it (Figure S5D). Fourth, the binding of Raptor, but not Rictor, to IRS-1 was detected (Figure 5F). These data suggest that mTORC1 is a major kinase for IRS-1 Ser 422. Considering the fact that Torin1, as well as rapamycin in the case of long-term treatment (Sarbassov et al., 2006), inhibits both mTORC1 and mTORC2, we also evaluated the effect of Rictor knockdown on IRS-1 Ser 422 phosphorylation. Rictor knockdown partially reduced it in IGF-I-stimulated cells (Figure 5E). In our assay, Rictor knockdown inhibited IGF-I-induced phosphorylation of Akt Ser 473, a target site by mTORC2, and also weakly inhibited phosphorylation of S6K1, indicating either a direct or an indirect (mTORC1-mediated) role of mTORC2 in IRS-1 phosphorylation. Further examination of mTORC2 contribution to IRS-1 Ser 422 phosphorylation is required. We also show that IRS-1 interacts with mTORC1 via the SAIN domain (Figures 5F and S5F). Although this interaction was not enhanced by IGF-I, mTORC1 was still active under serum starvation conditions in our setup as judged by S6K1 phosphorylation (Figure S5D), possibly explaining the detected interaction between IRS-1 and active mTORC1 under either unstimulated or stimulated conditions.

Both mTORC1 and S6K1 could phosphorylate IRS-1 *in vitro* (Harrington et al., 2004; Tzatsos and Kandror, 2006). We showed that IRS-1 degradation induced by prolonged IGF-I stimulation was inhibited by rapamycin and Torin1 but not by the S6K1 inhibitor PF-470861 (Figure 1). In addition, the pharmacological inhibition of S6K1 did not influence Ser 422 phosphorylation of IRS-1 in IGF-I-stimulated cells (Figure 5B), indicating the negligible role of S6K1 activity in IRS-1 degradation. In contrast, RNAi-mediated knockdown of S6K1/2 has reportedly rescued the decrease in IRS-1 protein abundance with the concomitant increase in IRS-1 mRNA expression in TSC2 knockout MEFs (Harrington et al., 2004). This indicates that rapid inhibition of S6K1 by PF-470861, as evident in ablated phosphorylation of its major substrate S6 (Figure 1A), may not influence IRS-1 transcription, whereas chronic inhibition of S6K1/2 by RNAi may affect IRS-1 transcription but not the protein degradation, resulting in the observed IRS-1 protein increase. Therefore, S6K1 is unlikely to trigger IRS-1 degradation under physiological conditions like persistent insulin/IGF stimuli, although S6K1 mediates a negative feedback in ways other than IRS-1 degradation as reportedly shown in S6K1 knockout mice (Um et al., 2004).

Although several RING-type E3 ligases have been reported to ubiquitinate IRS-1 (Nakao et al., 2009; Rui et al., 2002; Shi et al., 2011; Usui et al., 2004; Xu et al., 2008; Yi et al., 2013), none of them have been proved to induce mTORC1-dependent degradation of IRS-1 as a negative feedback regulator of insulin/IGF

signaling. The Cullin7/Fbxw8 complex has been reported to target Ser-phosphorylated IRS-1 (Kim et al., 2012; Xu et al., 2008). However, our study showed that neither knockdown of Cullin7 nor of Fbxw8 inhibited IRS-1 degradation induced by prolonged IGF-I stimulation (Figure 2B). Similar results have been shown by another group that used the skeletal muscle cell line C2C12 (Shi et al., 2011). In a report discovering the Cullin1-containing complex that targets IRS-1 for degradation, the RNAi screening has identified a skeletal-muscle-specific Fbxo40 as the F box protein required for IRS-1 degradation in the differentiated myotubes (Shi et al., 2011), which could not yet explain the IRS-1 degradation observed in other cell types. In this study we identified β-TRCP as the F box protein of the SCF complex responsible for IRS-1 degradation. β-TRCP is expressed ubiquitously (Frescas and Pagano, 2008; Wang et al., 2014). Importantly, the interaction of IRS-1 with β-TRCP is dependent on mTORC1-mediated phosphorylation of Ser 422, which was validated in L6 cells in this study. Although the roles of mTORC1 for the β-TRCP recruitment to IRS-1 and the IRS-1 degradation in other cell types remain to be determined, the regulation coupled with $SCF^{\beta\text{-}TRCP}$ and mTORC1 could be a common mechanism for IRS-1 degradation.

Many studies have revealed that constitutive activation of the mTORC1/S6K cascade, as exemplified in TSC1/2-depleted cells, blocks the PI3K/Akt signaling activated by insulin and IGF. This negative feedback includes inhibition of insulin/IGF-I receptor kinases by mTORC1-dependent stabilization of Grb10 (Hsu et al., 2011; Yu et al., 2011), inhibition of mTORC2 by mTORC1-dependent phosphorylation of Sin1 (Liu et al., 2013), and inhibition of IGF ligand ability by mTORC1-dependent induction of IGF-binding protein 5 (IGFBP5) secretion (Ding et al., 2016). Our study revealed how the degradation of IRS-1 contributes to the ablated sensitivity to insulin/IGF. Expression of the degradation-resistant IRS-1 S422A mutant in TSC2 knockout cells restored the sensitivity to IGF-I in part, which was confirmed by phosphorylation of Akt, DNA synthesis, and protection of starvation-induced apoptosis (Figure 6), suggesting that mTORC1-induced degradation of IRS-1 downregulates IGF-stimulated PI3K/Akt signaling in this context. As shown in Figure S1B, the effect of mTORC1 is not specific for IRS-1 Ser 422 but is also observed in other residues, including Ser 302, Ser 307, and Ser 318. It is worth noting that the sensitivity to IGF-I in TSC2 knockout cells was not restored when the non-degradation-resistant IRS-1 4SA mutant, in which known phosphosites Ser 302, Ser 307, Ser 318, and Ser 522 are mutated into Ala, was expressed at a level comparable with that of IRS-1 WT. Although phosphorylation of these Ser residues has been reported to negatively regulate IRS-1 function (Copps and White, 2012), degradation of IRS-1 via Ser 422 phosphorylation likely plays a predominant role in suppressing the signaling function of IRS-1 in the cells with constitutive mTORC1 activation (Figure S6B). Since TSC2 knockout cells expressing the IRS-1 S422A did not fully restore IGF signaling (Figure 6), other mechanisms should contribute to the mTORC1-mediated inhibition of IGF signaling. In particular, mTORC1-induced secretion of IGFBP5 is a possible candidate for this because our study used the same TSC2 knockout model as a previous study discovering the link between mTORC1 and IGFBP5 (Ding et al., 2016).

The stability of IRS-1 could reflect how long Akt activity is sustained upon IGF stimulation. In line with this, IGF-I-induced phosphorylation of Akt was more sustained when mTORC1-mediated degradation of IRS-1 was inhibited by two independent ways, knockdown of β-TRCP and expression of IRS-1 S422A (Figures 7A–7D). Several lines of evidence have demonstrated that the Akt signaling utilizes different temporal patterns in response to specific stimuli and decodes selective downstream substrates to regulate complex cellular behaviors (Gross and Rotwein, 2016; Kubota et al., 2012). Indeed, a mathematical modeling study has demonstrated that the Akt signaling to FoxO selectively responds to the sustainability but not the amplitude of Akt activity in response to the ligands (Kubota et al., 2012). Therefore, our study indicates that mTORC1-mediated control of IRS-1 degradation encodes the temporal Akt signaling, leading to selective regulation of insulin/IGF actions (Figure 7E).

Deregulation of the negative feedback loop between IRS-1 and the mTORC1 cascade appears to affect several pathogenic conditions. Obese or high-fat-diet-fed mice display elevated mTORC1 signaling and insulin resistance in various tissues, probably due to hyperinsulinemia and excessive nutrients such as amino acids (Khamzina et al., 2005). The enhanced mTORC1 cascade could induce peripheral insulin resistance because of the over-driving feedback inhibition of IRS-1. However, this model still has many challenges, as some reports have suggested that the upstream signaling defect, including IRS-1 degradation, is a consequence of insulin resistance rather than a cause (Hoehn et al., 2008). In addition, mTORC1-dependent suppression of insulin and mTORC2 signaling is an important hallmark of pancreatic β cells under conditions of increased β cell stress and metabolic demands in diabetes (Ardestani et al., 2018). Future studies

to determine whether obesity or metabolic stresses affect IRS-1 Ser 422 phosphorylation in insulin-sensitive tissues and β cells could address these issues. Hyperactivation of the mTORC1 cascades is a hallmark in many types of cancers (Menon and Manning, 2008). mTOR inhibitors have been in trial for anti-tumor drugs, but the relief of feedback inhibition of the PI3K/Akt pathway that occurs with mTORC1 inhibition paradoxically could activate Akt and promote cell survival, which may partly account for the limited success of mTOR inhibitors. In line with this idea, mTOR inhibitor treatment upregulates the PI3K/Akt signaling dependent on the insulin/IGF-I receptor pathway in different cancer cell lines (Rodrik-Outmezguine et al., 2011; Wan et al., 2007; Yoon et al., 2017). Although our study did not use cancer cells, these observations raise the idea of a potential role for the mTORC1-IRS-1 feedback cascade in cancer survival strategy, which should be tested in the appropriate model. Our study provides an experimental framework for understanding how mTORC1-mediated control of IRS-1 turnover contributes to insulin resistance and tumor resistance to mTOR inhibitors.

METHODS

All methods can be found in the accompanying Transparent Methods supplemental file.

SUPPLEMENTAL INFORMATION

Supplemental Information includes Transparent Methods, six figures, and two tables and can be found with this article online at https://doi.org/10.1016/j.isci.2018.06.006.

ACKNOWLEDGMENTS

We thank Dr. Toshiaki Fukushima (Tokyo Institute of Technology) for technical advice and valuable discussion. We also thank members of the Takahashi laboratory for valuable support and discussion and Dr. Susan Hall (University of North Carolina) for critically reading the manuscript. This work was supported in part by Grants-in-Aid for the Japan Society for the Promotion of Science (JSPS) Fellows and for Young Scientists (B) #15K18766 from JSPS to Y.Y.; Grant-in-Aid for Scientific Research (B) #17H03802 from JSPS to T.M.; Grant-in-Aid for Scientific Research (S) #25221204 and Scientific Research (A) #18H03972, and Core-to-core program A. A. Advanced Research Networks from JSPS to S.-I.T.

AUTHOR CONTRIBUTIONS

Y.Y., T.I., F.H., and S.-I. T. designed the experiments. Y.Y., T.I., and S.-I.I. performed the experiments. Y.Y., K.C., S.-I.I., T.N., T.M., F.H., and S.-I.T. contributed materials and analysis tools. Y.Y., F.H., and S.-I.T. wrote the paper.

DECLARATION OF INTERESTS

The authors declare no competing interests.

Received: February 12, 2018
Revised: May 3, 2018
Accepted: June 13, 2018
Published: July 27, 2018

REFERENCES

Ardestani, A., Lupse, B., Kido, Y., Leibowitz, G., and Maedler, K. (2018). mTORC1 signaling: a double-edged sword in diabetic β cells. Cell Metab. *27*, 314–331.

Berg, C.E., Lavan, B.E., and Rondinone, C.M. (2002). Rapamycin partially prevents insulin resistance induced by chronic insulin treatment. Biochem. Biophys. Res. Commun. *293*, 1021–1027.

Copps, K.D., and White, M.F. (2012). Regulation of insulin sensitivity by serine/threonine phosphorylation of insulin receptor substrate proteins IRS1 and IRS2. Diabetologia *55*, 2565–2582.

Ding, M., Bruick, R.K., and Yu, Y. (2016). Secreted IGFBP5 mediates mTORC1-dependent feedback inhibition of IGF-1 signalling. Nat. Cell Biol. *18*, 319–327.

Duda, D.M., Scott, D.C., Calabrese, M.F., Zimmerman, E.S., Zheng, N., and Schulman, B.A. (2011). Structural regulation of cullin-RING ubiquitin ligase complexes. Curr. Opin. Struct. Biol. *21*, 257–264.

Frescas, D., and Pagano, M. (2008). Deregulated proteolysis by the F-box proteins SKP2 and β-TrCP: tipping the scales of cancer. Nat. Rev. Cancer *8*, 438–449.

Gross, S.M., and Rotwein, P. (2016). Mapping growth-factor-modulated Akt signaling dynamics. J. Cell Sci. *129*, 2052–2063.

Harrington, L.S., Findlay, G.M., Gray, A., Tolkacheva, T., Wigfield, S., Rebholz, H., Barnett, J., Leslie, N.R., Cheng, S., Shepherd, P.R., et al. (2004). The TSC1-2 tumor suppressor controls insulin-PI3K signaling via regulation of IRS proteins. J. Cell Biol. *166*, 213–223.

Harrington, L.S., Findlay, G.M., and Lamb, R.F. (2005). Restraining PI3K: mTOR signalling goes back to the membrane. Trends Biochem. Sci. *30*, 35–42.

Hartley, D., and Cooper, G.M. (2002). Role of mTOR in the degradation of IRS-1: regulation of PP2A activity. J. Cell. Biochem. *85*, 304–314.

Haruta, T., Uno, T., Kawahara, J., Takano, A., Egawa, K., Sharma, P.M., Olefsky, J.M., and Kobayashi, M. (2000). A rapamycin-sensitive pathway down-regulates insulin signaling via phosphorylation and proteasomal degradation of insulin receptor substrate-1. Mol. Endocrinol. *14*, 783–794.

Hoehn, K.L., Hohnen-Behrens, C., Cederberg, A., Wu, L.E., Turner, N., Yuasa, T., Ebina, Y., and James, D.E. (2008). IRS1-independent defects define major nodes of insulin resistance. Cell Metab. *7*, 421–433.

Hornbeck, P.V., Zhang, B., Murray, B., Kornhauser, J.M., Latham, V., and Skrzypek, E. (2015). PhosphoSitePlus, 2014: mutations, PTMs and recalibrations. Nucleic Acids Res. *43*, D512–D520.

Hsu, P.P., Kang, S.A., Rameseder, J., Zhang, Y., Ottina, K.A., Lim, D., Peterson, T.R., Choi, Y., Gray, N.S., Yaffe, M.B., et al. (2011). The mTOR-regulated phosphoproteome reveals a mechanism of mTORC1-mediated inhibition of growth factor signaling. Science *332*, 1317–1322.

Huang, C., Thirone, A.C.P., Huang, X., and Klip, A. (2005). Differential contribution of insulin receptor substrates 1 versus 2 to insulin signaling and glucose uptake in L6 myotubes. J. Biol. Chem. *280*, 19426–19435.

Humphrey, S.J., Yang, G., Yang, P., Fazakerley, D.J., Stöckli, J., Yang, J.Y., and James, D.E. (2013). Dynamic adipocyte phosphoproteome reveals that Akt directly regulates mTORC2. Cell Metab. *17*, 1009–1020.

Inoki, K., Li, Y., Zhu, T., Wu, J., and Guan, K.-L. (2002). TSC2 is phosphorylated and inhibited by Akt and suppresses mTOR signalling. Nat. Cell Biol. *4*, 648–657.

Khamzina, L., Veilleux, A., Bergeron, S., and Marette, A. (2005). Increased activation of the mammalian target of rapamycin pathway in liver and skeletal muscle of obese rats: possible involvement in obesity-linked insulin resistance. Endocrinology *146*, 1473–1481.

Kim, D.-H., Sarbassov, D.D., Ali, S.M., King, J.E., Latek, R.R., Erdjument-Bromage, H., Tempst, P., and Sabatini, D.M. (2002). mTOR interacts with raptor to form a nutrient-sensitive complex that signals to the cell growth machinery. Cell *110*, 163–175.

Kim, S.J., DeStefano, M.A., Oh, W.J., Wu, C., Vega-Cotto, N.M., Finlan, M., Liu, D., Su, B., and Jacinto, E. (2012). mTOR complex 2 regulates proper turnover of insulin receptor Substrate-1 via the ubiquitin ligase subunit Fbw8. Mol. Cell *48*, 875–887.

Kubota, H., Noguchi, R., Toyoshima, Y., Ozaki, Y., Uda, S., Watanabe, K., Ogawa, W., and Kuroda, S. (2012). Temporal coding of insulin action through multiplexing of the AKT pathway. Mol. Cell *46*, 820–832.

Lee, A.V., Gooch, J.L., Oesterreich, S., Guler, R.L., and Yee, D. (2000). Insulin-like growth factor I-induced degradation of insulin receptor substrate 1 is mediated by the 26S proteasome and blocked by phosphatidylinositol 3′-kinase inhibition. Mol. Cell. Biol. *20*, 1489–1496.

Liu, P., Gan, W., Inuzuka, H., Lazorchak, A.S., Gao, D., Arojo, O., Liu, D., Wan, L., Zhai, B., Yu, Y., et al. (2013). Sin1 phosphorylation impairs mTORC2 complex integrity and inhibits downstream Akt signalling to suppress tumorigenesis. Nat. Cell Biol. *15*, 1340–1350.

Ma, X.M., and Blenis, J. (2009). Molecular mechanisms of mTOR-mediated translational control. Nat. Rev. Mol. Cell Biol. *10*, 307–318.

Manning, B.D., and Cantley, L.C. (2007). AKT/PKB signaling: navigating downstream. Cell *129*, 1261–1274.

Manning, B.D., Tee, A.R., Logsdon, M.N., Blenis, J., and Cantley, L.C. (2002). Identification of the tuberous sclerosis complex-2 tumor suppressor gene product tuberin as a target of the phosphoinositide 3-kinase/Akt pathway. Mol. Cell *10*, 151–162.

Menon, S., Dibble, C.C., Talbott, G., Hoxhaj, G., Valvezan, A.J., Takahashi, H., Cantley, L.C., and Manning, B.D. (2014). Spatial control of the TSC complex integrates insulin and nutrient regulation of mTORC1 at the lysosome. Cell *156*, 771–785.

Menon, S., and Manning, B.D. (2008). Common corruption of the mTOR signaling network in human tumors. Oncogene *27*, S43–S51.

Myers, M.G., Zhang, Y., Aldaz, G.A., Grammer, T., Glasheen, E.M., Yenush, L., Wang, L.M., Sun, X.J., Blenis, J., Pierce, J.H., and White, M.F. (1996). YMXM motifs and signaling by an insulin receptor substrate 1 molecule without tyrosine phosphorylation sites. Mol. Cell. Biol. *16*, 4147–4155.

Nakae, J., Kido, Y., and Accili, D. (2001). Distinct and overlapping functions of insulin and IGF-I receptors. Endocr. Rev. *22*, 818–835.

Nakao, R., Hirasaka, K., Goto, J., Ishidoh, K., Yamada, C., Ohno, A., Okumura, Y., Nonaka, I., Yasutomo, K., Baldwin, K.M., et al. (2009). Ubiquitin ligase Cbl-b is a negative regulator for insulin-like growth factor 1 signaling during muscle atrophy caused by unloading. Mol. Cell. Biol. *29*, 4798–4811.

Ohne, Y., Takahara, T., Hatakeyama, R., Matsuzaki, T., Noda, M., Mizushima, N., and Maeda, T. (2008). Isolation of hyperactive mutants of mammalian target of rapamycin. J. Biol. Chem. *283*, 31861–31870.

Pearce, L.R., Alton, G.R., Richter, D.T., Kath, J.C., Lingardo, L., Chapman, J., Hwang, C., and Alessi, D.R. (2010). Characterization of PF-4708671, a novel and highly specific inhibitor of p70 ribosomal S6 kinase (S6K1). Biochem. J. *431*, 245–255.

Rodrik-Outmezguine, V.S., Chandarlapaty, S., Pagano, N.C., Poulikakos, P.I., Scaltriti, M., Moskatel, E., Baselga, J., Guichard, S., and Rosen, N. (2011). mTOR kinase inhibition causes feedback-dependent biphasic regulation of AKT signaling. Cancer Discov. *1*, 248–259.

Rui, L., Yuan, M., Frantz, D., Shoelson, S., and White, M.F. (2002). SOCS-1 and SOCS-3 block insulin signaling by ubiquitin-mediated degradation of IRS1 and IRS2. J. Biol. Chem. *277*, 42394–42398.

Sarbassov, D.D., Ali, S.M., Sengupta, S., Sheen, J.-H., Hsu, P.P., Bagley, A.F., Markhard, A.L., and Sabatini, D.M. (2006). Prolonged rapamycin treatment inhibits mTORC2 assembly and Akt/PKB. Mol. Cell *22*, 159–168.

Saxton, R.A., and Sabatini, D.M. (2017). mTOR signaling in growth, metabolism, and disease. Cell *168*, 960–976.

Shah, O.J., Wang, Z., and Hunter, T. (2004). Inappropriate activation of the TSC/Rheb/mTOR/S6K cassette induces IRS1/2 depletion, insulin resistance, and cell survival deficiencies. Curr. Biol. *14*, 1650–1656.

Shi, J., Luo, L., Eash, J., Ibebunjo, C., and Glass, D.J. (2011). The SCF-Fbxo40 complex induces IRS1 ubiquitination in skeletal muscle, limiting IGF1 signaling. Dev. Cell *21*, 835–847.

Sun, X.J., Crimmins, D.L., Myers, M.G., Miralpeix, M., and White, M.F. (1993). Pleiotropic insulin signals are engaged by multisite phosphorylation of IRS-1. Mol. Cell. Biol. *13*, 7418–7428.

Tzatsos, A. (2009). Raptor binds the SAIN (Shc and IRS-1 NPXY binding) domain of insulin receptor substrate-1 (IRS-1) and regulates the phosphorylation of IRS-1 at Ser-636/639 by mTOR. J. Biol. Chem. *284*, 22525–22534.

Tzatsos, A., and Kandror, K.V. (2006). Nutrients suppress phosphatidylinositol 3-kinase/Akt signaling via raptor-dependent mTOR-mediated insulin receptor substrate 1 phosphorylation. Mol. Cell. Biol. *26*, 63–76.

Um, S.H., Frigerio, F., Watanabe, M., Picard, F., Joaquin, M., Sticker, M., Fumagalli, S., Allegrini, P.R., Kozma, S.C., Auwerx, J., and Thomas, G. (2004). Absence of S6K1 protects against age- and diet-induced obesity while enhancing insulin sensitivity. Nature *431*, 200–205.

Usui, I., Imamura, T., Huang, J., Satoh, H., Shenoy, S.K., Lefkowitz, R.J., Hupfeld, C.J., and Olefsky, J.M. (2004). β-arrestin-1 competitively inhibits insulin-induced ubiquitination and degradation of insulin receptor substrate 1. Mol. Cell. Biol. *24*, 8929–8937.

Wan, X., Harkavy, B., Shen, N., Grohar, P., and Helman, L.J. (2007). Rapamycin induces feedback activation of Akt signaling through an IGF-1R-dependent mechanism. Oncogene *26*, 1932–1940.

Wang, Z., Liu, P., Inuzuka, H., and Wei, W. (2014). Roles of F-box proteins in cancer. Nat. Rev. Cancer *14*, 233–247.

White, M.F. (2002). IRS proteins and the common path to diabetes. Am. J. Physiol. Endocrinol. Metab. *283*, E413–E422.

Wu, G., Xu, G., Schulman, B.A., Jeffrey, P.D., Harper, J.W., and Pavletich, N.P. (2003). Structure of a β-TrCP1-Skp1-β-Catenin complex: destruction motif binding and lysine specificity of the SCF(β-TrCP1) ubiquitin ligase. Mol. Cell *11*, 1445–1456.

Xu, X., Sarikas, A., Dias-Santagata, D.C., Dolios, G., Lafontant, P.J., Tsai, S.-C., Zhu, W., Nakajima, H., Nakajima, H.O., Field, L.J., et al. (2008). The CUL7 E3 ubiquitin ligase targets insulin receptor substrate 1 for ubiquitin-dependent degradation. Mol. Cell *30*, 403–414.

Yi, J.-S., Park, J.S., Ham, Y.-M., Nguyen, N., Lee, N.-R., Hong, J., Kim, B.-W., Lee, H., Lee, C.-S., Jeong, B.-C., et al. (2013). MG53-induced IRS-1 ubiquitination negatively regulates skeletal myogenesis and insulin signalling. Nat. Commun. *4*, 2354.

Yoneyama, Y., Lanzerstorfer, P., Niwa, H., Umehara, T., Shibano, T., Yokoyama, S., Chida, K., Weghuber, J., Hakuno, F., and Takahashi, S.-I. (2018). IRS-1 acts as an endocytic regulator of IGF-I receptor to facilitate sustained IGF signaling. Elife *7*, https://doi.org/10.7554/eLife.32893.

Yoneyama, Y., Matsuo, M., Take, K., Kabuta, T., Chida, K., Hakuno, F., and Takahashi, S.-I. (2013). The AP-1 complex regulates intracellular localization of insulin receptor substrate 1, which is required for insulin-like growth factor I-dependent cell proliferation. Mol. Cell. Biol. *33*, 1991–2003.

Yoon, S.-O., Shin, S., Karreth, F.A., Buel, G.R., Jedrychowski, M.P., Plas, D.R., Dedhar, S., Gygi, S.P., Roux, P.P., Dephoure, N., and Blenis, J. (2017). Focal adhesion- and IGF1R-dependent survival and migratory pathways mediate tumor resistance to mTORC1/2 inhibition. Mol. Cell *67*, 512–527.

Yu, Y., Yoon, S.-O., Poulogiannis, G., Yang, Q., Ma, X.M., Villén, J., Kubica, N., Hoffman, G.R., Cantley, L.C., Gygi, S.P., and Blenis, J. (2011). Phosphoproteomic analysis identifies Grb10 as an mTORC1 substrate that negatively regulates insulin signaling. Science *332*, 1322–1326.

ISCI, Volume *5*

Supplemental Information

Serine Phosphorylation by mTORC1 Promotes IRS-1 Degradation through SCFβ-TRCP E3 Ubiquitin Ligase

Yosuke Yoneyama, Tomomi Inamitsu, Kazuhiro Chida, Shun-Ichiro Iemura, Tohru Natsume, Tatsuya Maeda, Fumihiko Hakuno, and Shin-Ichiro Takahashi

Supplemental Figures

Figure S1

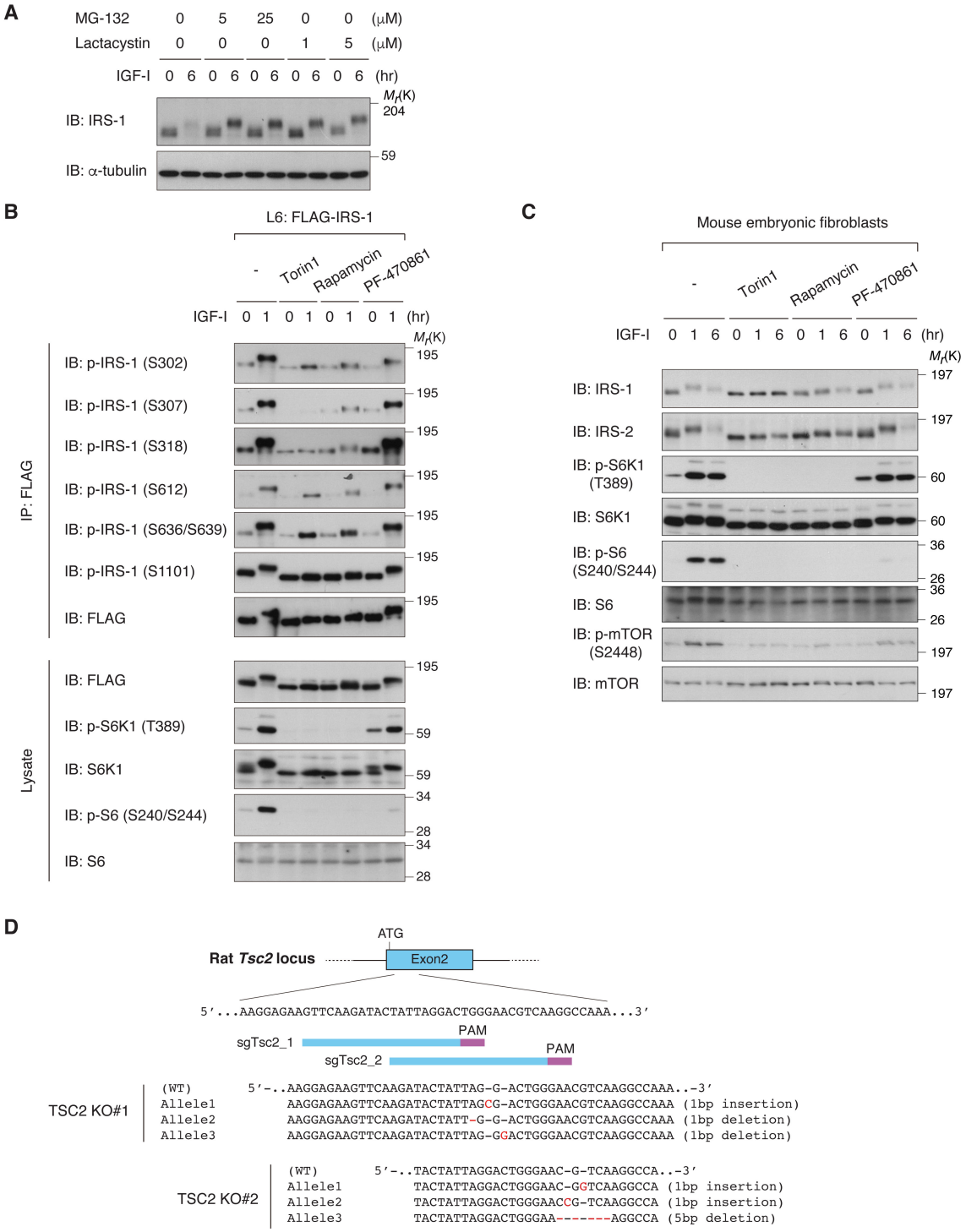

Figure S1. Multiple Ser phosphorylation of IRS-1 shows differential responses to the mTOR pathway inhibitors in IGF-I-stimulated cells. Related to Figure 1.

(A) Immunoblot (IB) analysis of whole cell lysates derived from L6 cells that were serum-starved, treated with the indicated proteasome inhibitors (MG-132 and Lactacystin), and then collected at the indicated time periods following IGF-I stimulation.

(B) L6 cells stably expressing FLAG-IRS-1 (L6: FLAG-IRS-1) were serum-starved, treated with the indicated inhibitors, and then collected at the indicated time periods following IGF-I stimulation. FLAG-IRS-1 proteins were immunoprecipitated (IP), and the immunoprecipitated IRS-1 phosphorylation and S6K1/S6 phosphorylation were analyzed by immunoblotting with the indicated antibodies.

(C) Immunoblot analysis of whole cell lysates derived from MEFs that were serum-starved, treated with the indicated inhibitors, and then collected at the indicated time periods following IGF-I stimulation.

(D) Schematic representation of base pairing between the sgRNAs and the targeting locus of Exon 2 in the rat *Tsc2* gene. The sequences of the mutated alleles in *Tsc2* in two independent clones are shown.

The data shown are representative of three independent experiments.

Figure S2

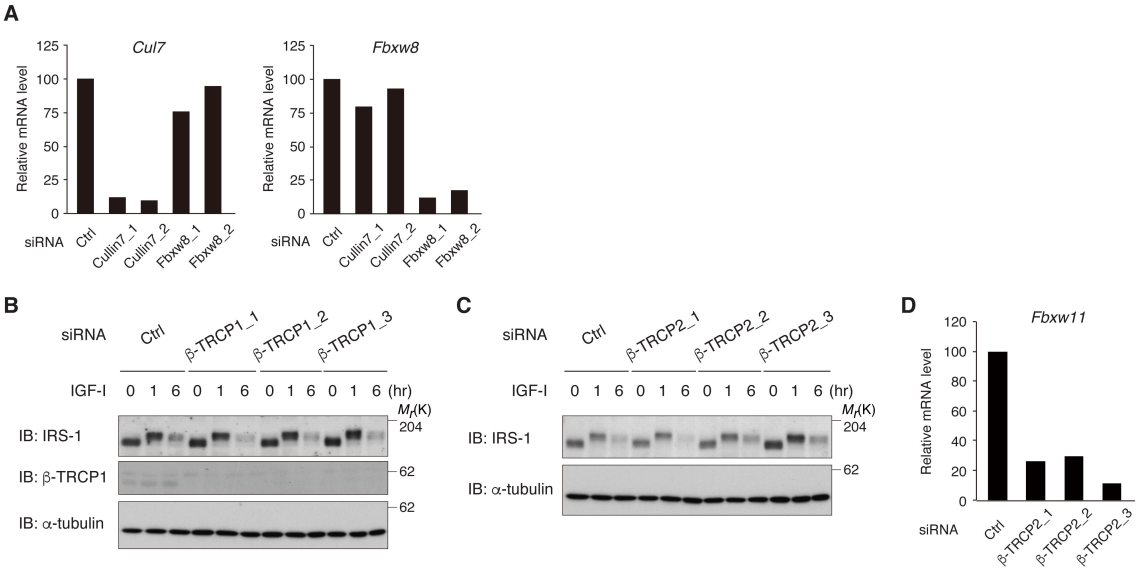

Figure S2. Single knockdown of β-TRCP1 or β-TRCP2 has minor effects on IRS-1 degradation induced by prolonged IGF-I stimulation. Related to Figure 2.

(A) Quantitative RT-PCR analysis of *Cul7* and *Fbxw8* mRNA levels from L6 cell transfected with siRNA targeting Cullin7 or Fbxw8. The expression level of each gene was normalized to the *Gapdh* gene. Data are expressed as fold of the value in cells transfected with control siRNA.

(B and C) L6 cells were transfected with siRNA targeting either β-TRCP1 (B) or β-TRCP2 (C), serum-starved, and then collected at the indicated time periods following IGF-I stimulation. The cell lysates were subjected to immunoblotting (IB) with the indicated antibodies.

(D) Quantitative RT-PCR analysis of *Fbxw11* (β-TRCP2) mRNA levels from L6 cell transfected with siRNA targeting β-TRCP2. The expression level of each gene was normalized to the *Gapdh* gene. Data are expressed as fold of the value in cells transfected with control siRNA.

The data shown are representative of three independent experiments.

Figure S3

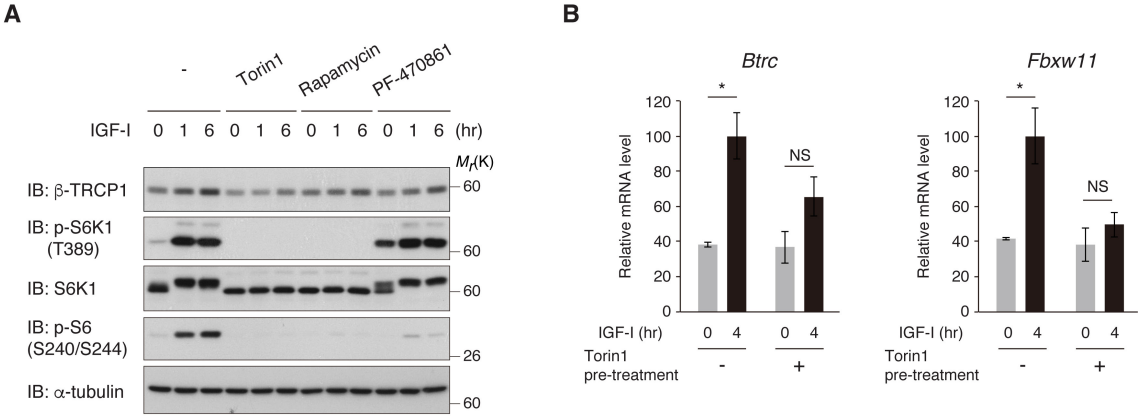

Figure S3. IGF-I increases the β-TRCP expression in an mTOR-dependent manner. Related to Figure 2 and Figure 3.

(A) Immunoblot (IB) analysis of whole cell lysates derived from L6 cells that were serum-starved, treated with the indicated inhibitors, and then collected at the indicated time periods following IGF-I stimulation.

(B) Quantitative RT-PCR analysis of *Btrc* (β-TRCP1) and *Fbxw11* (β-TRCP2) mRNA levels from L6 cell that were serum-starved, treated with or without Torin1, and then collected at the indicated time periods following IGF-I stimulation. The expression level of each gene was normalized to the *Rn18s* gene. Data are expressed as fold of the value in cells transfected with control siRNA.

The data shown are representative of two independent experiments.

Figure S4

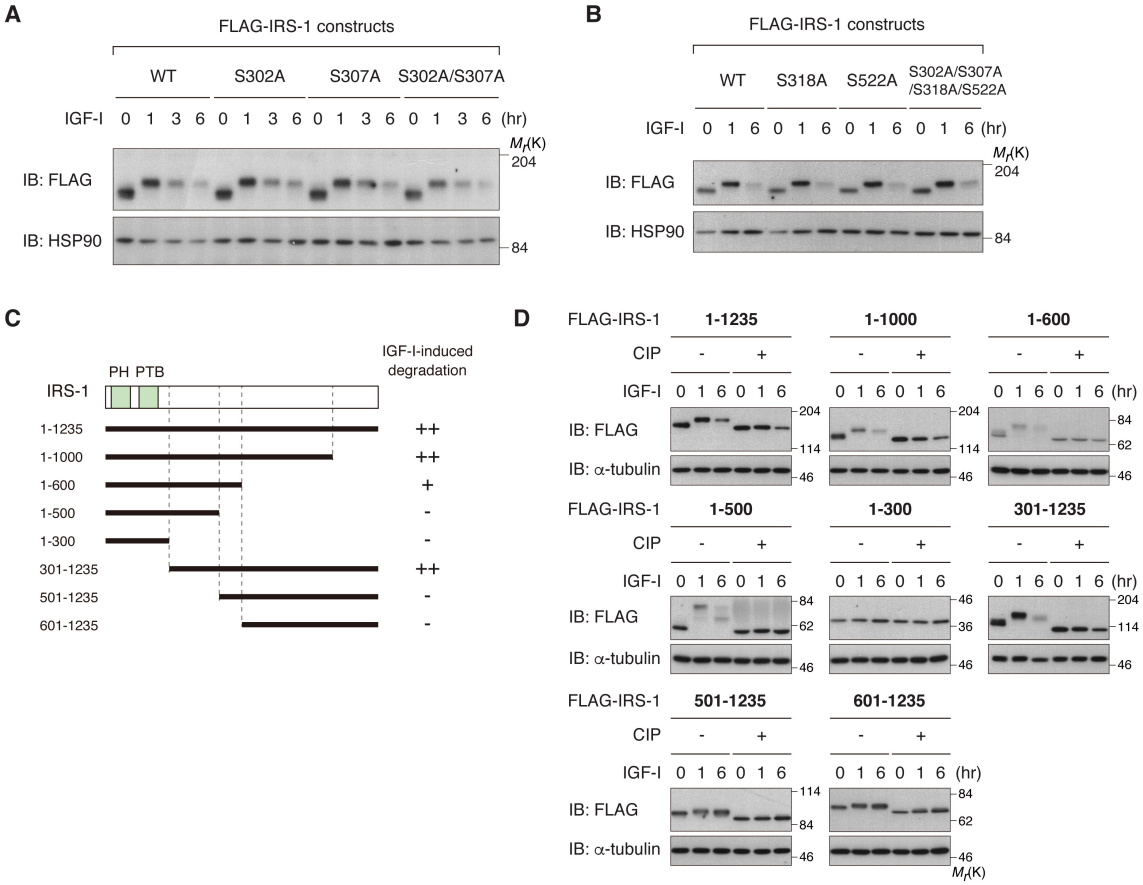


```
WT             301 ESITATSPASMVGGKPGSFRVRASSDGEGTMSRPASVDGSPVSPSTNRTHAHRHRGSSRL 360
STA(301-600)   301 EAIAAAAPAAMVGGKPGAFRVRAAADGEGTMARPAAVDGAPVAPAANRTHAHRHRGAARL 360
STA(301-500)   301 EAIAAAAPAAMVGGKPGAFRVRAAADGEGTMARPAAVDGAPVAPAANRTHAHRHRGAARL 360
STA(501-600)   301 ESITATSPASMVGGKPGSFRVRASSDGEGTMSRPASVDGSPVSPSTNRTHAHRHRGSSRL 360

WT             361 HPPLNHSRSIPMPSSRCSPSATSPVSLSSSSTSGHGSTSDCLFPRRSSASVSGSPSDGGF 420
STA(301-600)   361 HPPLNHARAIPMPSSRCAPAATAPVALSSSSTSGHGSTSDCLFPRRAAASVAGAPSDGGF 420
STA(301-500)   361 HPPLNHARAIPMPSSRCAPAATAPVALSSSSTSGHGSTSDCLFPRRAAASVAGAPSDGGF 420
STA(501-600)   361 HPPLNHSRSIPMPSSRCSPSATSPVSLSSSSTSGHGSTSDCLFPRRSSASVSGSPSDGGF 420

WT             421 ISSDEYGSSPCDFRSSFRSVTPDSLGHTPPARGEEELSNYICMGGKGASTLTAPNGHYIL 480
STA(301-600)   421 IAADEYGSSPCDFRSAFRAVAPDALGHAPPARGEEELANYICMGGKGASTLTAPNGHYIL 480
STA(301-500)   421 IAADEYGSSPCDFRSAFRAVAPDALGHAPPARGEEELANYICMGGKGASTLTAPNGHYIL 480
STA(501-600)   421 ISSDEYGSSPCDFRSSFRSVTPDSLGHTPPARGEEELSNYICMGGKGASTLTAPNGHYIL 480

WT             481 SRGGNGHRYIPGATMGTSPALTGDEAAGAADLDNRFRKRTHSAGTSPTISHQKTPSQSSV 540
STA(301-600)   481 ARGGNGHRYIPGATMGAAPALAGDEAAGAADLDNRFRKRAHAAGAAPAIAHQKTPSQSSV 540
STA(301-500)   481 ARGGNGHRYIPGATMGAAPALTGDEAAGAADLDNRFRKRTHSAGTSPTISHQKTPSQSSV 540
STA(501-600)   481 SRGGNGHRYIPGATMGTSPALAGDEAAGAADLDNRFRKRAHAAGAAPAIAHQKTPSQSSV 540

WT             541 VSIEEYTEMMPAAYPPGGGSGGRLPGYRHSAFVPTHSYPEEGLEMHHLERRGGHHRPDSS 600
STA(301-600)   541 VSIEEYTEMMPAAYPPGGGSGGRLPGYRHAAFVPTHAYPEEGLEMHHLERRGGHHRPDAA 600
STA(301-500)   541 VSIEEYTEMMPAAYPPGGGSGGRLPGYRHSAFVPTHSYPEEGLEMHHLERRGGHHRPDSS 600
STA(501-600)   541 VSIEEYTEMMPAAYPPGGGSGGRLPGYRHAAFVPTHAYPEEGLEMHHLERRGGHHRPDAA 600
```

Figure S4. Mapping of the degron-containing region in IRS-1. Related to Figure 4.

(A and B) Immunoblot (IB) analysis of whole cell lysates derived from L6 cells stably expressing the indicated FLAG-IRS-1 mutants that were serum-starved and then collected at the indicated time periods following IGF-I stimulation.

(C) Schematic illustration of the IRS-1 deletion mutants used in (D).

(D) Immunoblot analysis of whole cell lysates derived from L6 cells stably expressing the indicated FLAG-IRS-1 deletion mutants that were serum-starved and then collected at the indicated time periods following IGF-I stimulation. The cell lysates were also treated with calf intestine alkaline phosphatase (CIP) to compare the amount of dephosphorylated IRS-1 mutants.

(E) Schematic illustration of the IRS-1 mutants in which potentially phosphorylated Ser/Thr residues in IRS-1 are substituted into Ala. The residues mutated to Ala are shown in red in the amino acid sequence of IRS-1.

The data shown are representative of three independent experiments.

Figure S5

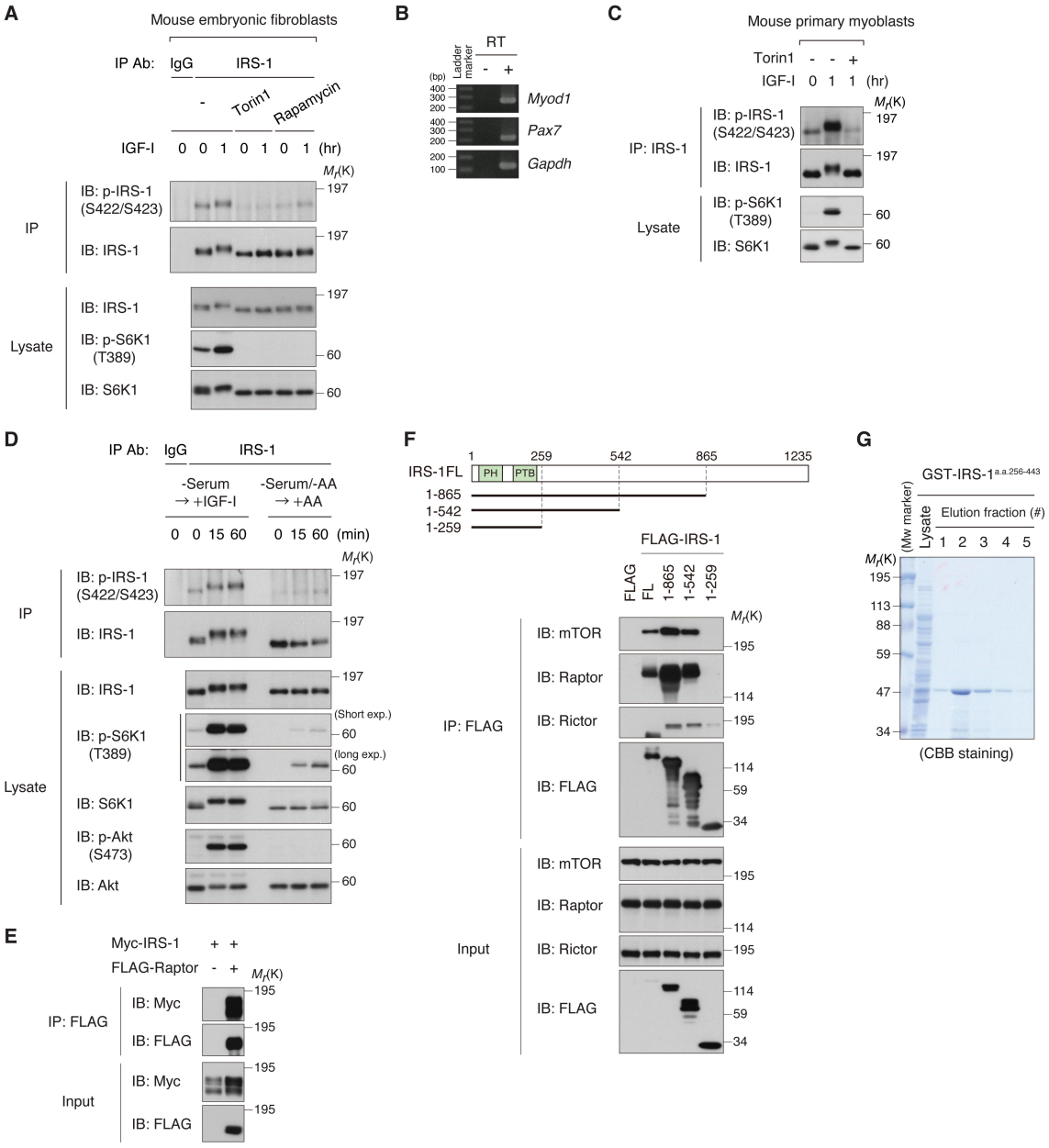

Figure S5. mTORC1 interacts with and phosphorylates IRS-1. Related to Figure 5. (A) MEFs were serum-starved, treated with the indicated inhibitors, and then collected at the indicated time periods following IGF-I stimulation. The endogenous IRS-1 proteins were immunoprecipitated (IP). The immunoprecipitated IRS-1 phosphorylation and S6K1 phosphorylation were analyzed by immunoblotting (IB) with the indicated

antibodies. The data shown are representative of two independent experiments.

(B and C) RT-PCR analysis of proliferating myoblast markers (*Myod1* and *Pax7*) and *Gapdh* gene expression in primary mouse myoblasts (B). Primary mouse myoblasts were serum-starved, treated with or without Torin1, and then collected at the indicated time periods following IGF-I stimulation. The endogenous IRS-1 proteins were immunoprecipitated. The immunoprecipitated IRS-1 phosphorylation and S6K1 phosphorylation were analyzed by immunoblotting with the indicated antibodies (C). The data are derived from a single experiment.

(D) L6 cells were serum-starved with or without amino acids prior to the stimulation with IGF-I or amino acids for the indicated time. The endogenous IRS-1 proteins were immunoprecipitated. The immunoprecipitated IRS-1 phosphorylation and S6K1/Akt phosphorylation were analyzed by immunoblotting with the indicated antibodies. The data shown are representative of two independent experiments.

(E) HEK293T cells were transfected with Myc-IRS-1 together with FLAG-Raptor or empty vector, and lysates were subjected to anti-FLAG immunoprecipitation and immunoblotting with the indicated antibodies. The data shown are representative of three independent experiments.

(F) HEK293T cells were transfected with the indicated FLAG-IRS-1 deletion mutants, and lysates were subjected to anti-FLAG immunoprecipitation and immunoblotting with the indicated antibodies. The data shown are representative of two independent experiments.

(G) Purification of GST-IRS-1$^{a.a.256\text{-}443}$ recombinant protein from *Escherichia coli* used for *in vitro* kinase assay shown in Figure 5G. The purified fractions were subjected to SDS-PAGE and Coomassie Brilliant Blue (CBB) staining.

Figure S6

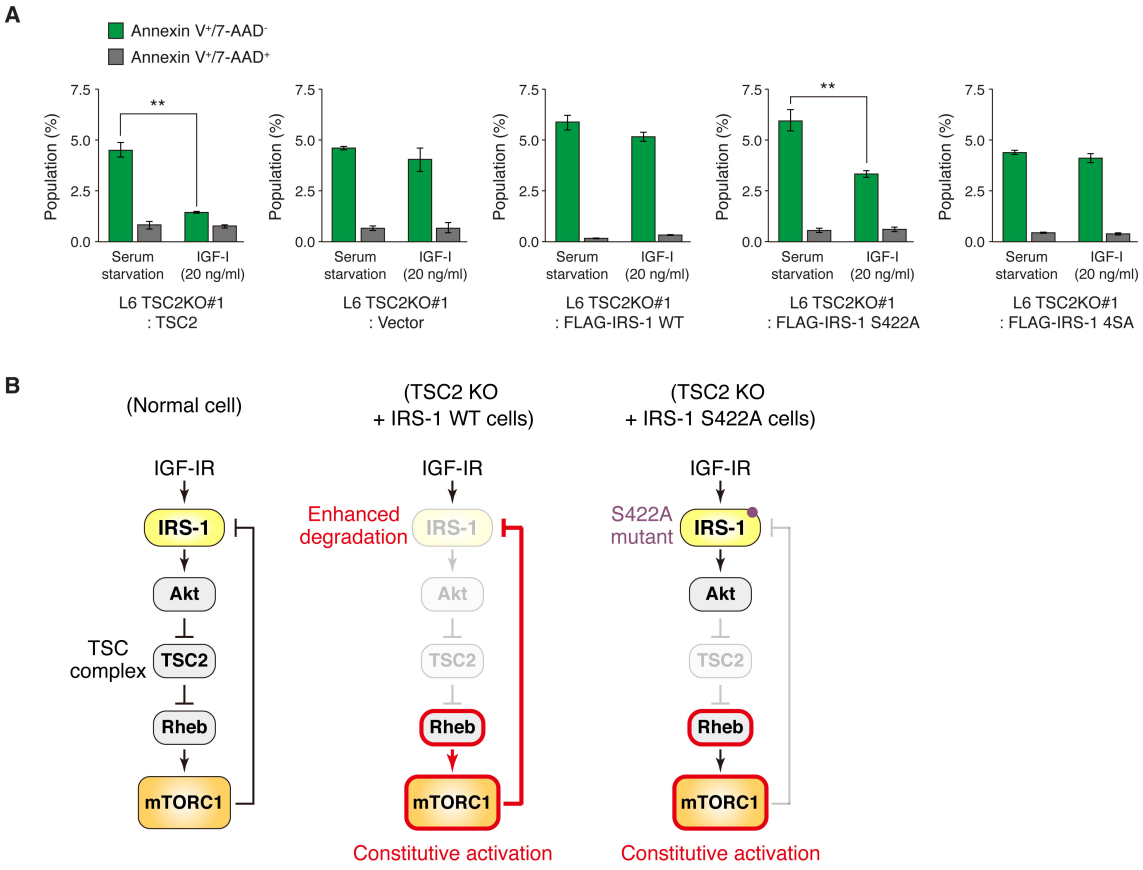

Figure S6. Expression of IRS-1 S422A mutant restores cell survival response to IGF-I in cells lacking TSC2. Related to Figure 6.

(A) L6 TSC2 KO cells stably expressing TSC2, FLAG-IRS-1 WT, S422A, 4SA, or empty vector were placed in serum-free medium with or without IGF-I (20 ng/ml) for 6 hr. The harvested cells were stained with Annexin V-FTIC and 7-AAD, and the stained cells were analyzed by flow cytometry. Results represent the percentage of Annexin $V^+/7\text{-}AAD^-$ (green bar) and Annexin $V^+/7\text{-}AAD^+$ (grey bar) to total cells (mean ± SEM; n=3; **P*<0.05). The data are representative of three independent experiments.

(B) Model illustrating the effect of IRS-1 S422A expression on IGF signaling in TSC2 knockout cells. In the TSC2 knockout cells, constitutive elevation of mTORC1 feedback signaling results in enhanced degradation of IRS-1, which leads to inability of Akt to activate in response to IGF-I. IRS-1 S422A escapes the mTORC1-mediated degradation in TSC2 knockout cells, which in turn restores the responsiveness to IGF-I

and activates the Akt signaling.

Table S1. Plasmids used in this study. Related to Figure 1–7

Plasmid designation	Insert	Source
pFLAG-CMV	(Empty vector)	
pFLAG-CMV-IRS-1	Rat IRS-1 full-length	(Fukushima *et al*, 2011)
pFLAG-CMV-IRS-1 1-865	Rat IRS-1 (a.a.1-865)	This study
pFLAG-CMV-IRS-1 1-542	Rat IRS-1 (a.a.1-542)	This study
pFLAG-CMV-IRS-1 1-259	Rat IRS-1 (a.a.1-259)	This study
pCMV5-Myc	(Empty vector)	
pCMV5-Myc-IRS-1	Rat IRS-1 full-length	This study
pFLAG-CMV-SOCS3	Human SOCS3	This study
pFLAG-CMV-Cul1	Human Cullin1	This study
pFLAG-CMV-Cul7	Human Cullin7	This study
pFLAG-CMV-Mdm2	Rat Mdm2	This study
pFLAG-CMV-Fbxw8	Human Fbxw8	This study
pFLAG-CMV-β-TRCP1	Human β-TRCP1	This study
pFLAG-CMV-β-TRCP2	Human β-TRCP2	This study
pFLAG-CMV-β-TRCP2 R423A	Human β-TRCP2 R423A	This study
pFLAG-CMV-Fbxo40	Rat Fbxo40	This study
pFLAG-CMV-Raptor	Rat Raptor	This study
pFLAG-CMV-GFP	GFP	This study
pcDNA3.1-FLAG-mTOR^{SL1+IT}	Rat mTOR	(Ohne *et al*, 2008)
pMXs-Puro	(Empty vector)	
pMXs-Puro-FLAG-IRS-1	FLAG-IRS-1 (rat)	This study
pMXs-Puro-FLAG-IRS-1 1-1000	FLAG-IRS-1 (a.a.1-1000)	This study
pMXs-Puro-FLAG-IRS-1 1-600	FLAG-IRS-1 (a.a.1-600)	This study
pMXs-Puro-FLAG-IRS-1 1-500	FLAG-IRS-1 (a.a.1-500)	This study
pMXs-Puro-FLAG-IRS-1 1-300	FLAG-IRS-1 (a.a.1-300)	This study
pMXs-Puro-FLAG-IRS-1 301-1235	FLAG-IRS-1 (a.a.301-1235)	This study
pMXs-Puro-FLAG-IRS-1 501-1235	FLAG-IRS-1 (a.a.501-1235)	This study

pMXs-Puro-FLAG-IRS-1 601-1235	FLAG-IRS-1 (a.a.601-1235)	This study
pMXs-Puro-FLAG-IRS-1 STA(301-600)	FLAG-IRS-1 (48×S/T->A in a.a.301-600)	This study
pMXs-Puro-FLAG-IRS-1 STA(301-500)	FLAG-IRS-1 (37×S/T->A in a.a.301-500)	This study
pMXs-Puro-FLAG-IRS-1 STA(501-600)	FLAG-IRS-1 (11×S/T->A in a.a.501-600)	This study
pMXs-Puro-FLAG-IRS-1 S302A	FLAG-IRS-1 S302A	This study
pMXs-Puro-FLAG-IRS-1 S307A	FLAG-IRS-1 S307A	This study
pMXs-Puro-FLAG-IRS-1 S318A	FLAG-IRS-1 S318A	This study
pMXs-Puro-FLAG-IRS-1 S522A	FLAG-IRS-1 S522A	This study
pMXs-Puro-FLAG-IRS-1 S302A/S307A	FLAG-IRS-1 S302A/S307A	This study
pMXs-Puro-FLAG-IRS-1 S302A/S307A/S318A/S512A	FLAG-IRS-1 S302A/S307A/S318A/S512A	This study
pMXs-Puro-FLAG-IRS-1 S325A/S332A	FLAG-IRS-1 S325A/S332A	This study
pMXs-Puro-FLAG-IRS-1 S407A/S408A	FLAG-IRS-1 S407A/S408A	This study
pMXs-Puro-FLAG-IRS-1 S412A/S414A	FLAG-IRS-1 S412A/S414A	This study
pMXs-Puro-FLAG-IRS-1 S422A/S423A	FLAG-IRS-1 S422A/S423A	This study
pMXs-Puro-FLAG-IRS-1 8SA	FLAG-IRS-1 S325A/S332A/S407A /S408A/S412A/S414A/S422A/S423A	This study
pMXs-Puro-FLAG-IRS-1 S416A	FLAG-IRS-1 S416A	This study
pMXs-Puro-FLAG-IRS-1 S422A	FLAG-IRS-1 S422A	This study
pMXs-Puro-FLAG-IRS-1 S423A	FLAG-IRS-1 S423A	This study
pMXs-Puro-TSC2	Rat TSC2	This study
pGEX-4T-1	(Empty vector)	
pGEX-IRS-1 256-443	Rat IRS-1 (a.a.256-443)	This study
pGEX-4EBP1	Rat 4EBP1	This study
pCS2-FN-Cas9-N-P2A-Puro	FLAG-NLS-SpCas9-NLS-P2A-Puro	This study
pCS2-U6-sgTsc2#1- FN-Cas9-N-P2A-Puro	U6-sgTsc2 #1 and FN-Cas9-N-P2A-Puro	This study
pCS2-U6-sgTsc2#2- FN-Cas9-N-P2A-Puro	U6-sgTsc2 #2 and FN-Cas9-N-P2A-Puro	This study

Table S2. siRNAs used in this study. Related to Figure 1–7

siRNA designation	Sequence
Control siRNA	5’-GUACCGCACGUCAUUCGUAUC-3’
Cullin1_1 siRNA	5’-CAUGCUACCGCACUUAAAUCA-3’
Cullin1_2 siRNA	5’-CGCAGUUACCAACGGUUUACA-3’
Cullin7_1 siRNA	5’-CUUCAAAGAUCGCAGAGUUCU-3’
Cullin7_2 siRNA	5’-GUUCUAUGCAGUCCCUAUAAC-3’
Fbxw8_1 siRNA	5’-GGCAUGUAGCCUCGGAAUUUG-3’
Fbxw8_2 siRNA	5’-GGUGUCACCUCAUGUAGAAGU-3’
β-TRCP1_1 siRNA	5’-CGCCUGUUUGCAGUACAGAGA-3’
β-TRCP1_2siRNA	5’-GAGACAGAACCAUAAAGGUGU-3’
β-TRCP1_3 siRNA	5’-GGUCAGAGUCUGAUCAAGUGG-3’
β-TRCP2_1 siRNA	5’-GUACAUAACGAUUCAAGCUCA-3’
β-TRCP2_2 siRNA	5’-GGGAUCAGUACCUGUUUAAAA-3’
β-TRCP2_3 siRNA	5’-CUAUCACAUGCCUAAGGGAGU-3’
β-TRCP1+2_A siRNA	β-TRCP1_1 siRNA + β-TRCP2_1 siRNA
β-TRCP1+2_B siRNA	β-TRCP1_2 siRNA + β-TRCP2_2 siRNA
Raptor_1 siRNA	5’-GCGAUCAAAGCAUUAGUCACA-3’
Raptor_2 siRNA	5’-GCUUGACUCCAGUUCGAGACA-3’
Rictor_1 siRNA	5’-GUUGUACACCCUUCUCAUAAU-3’
Rictor_2 siRNA	5’-GUACUAUUGAUAAUUAAUAAU-3’

Transparent Methods

Antibodies

Anti-phospho-IRS-1 (S422/S423) antibody was generated by immunizing rabbits with the synthetic peptide corresponding to the residues 419-GFI(pS)(pS)DEYG-427 of rat IRS-1. The antiserum obtained from the immunized rabbit was affinity-purified with a column conjugated with a phospho-peptide (GFI(pS)(pS)DEYG) for positive selection, and then bound fractions were applied to a column conjugated with a non-phospho-peptide (GFISSDEYG) for negative selection, and flow-through fractions were collected and used in this study (SCRUM Inc., Tokyo, Japan). Anti-phospho-4EBP1 (Thr37/46) antibody (2855), anti-Akt antibody (9272), anti-phospho-Akt (Thr308) antibody (9275), anti-phospho-Akt (Ser473) antibody (9271), anti-β-TRCP1 antibody (4394), anti-Caspase-3 antibody (9662), anti-Cullin1 antibody (4995), anti-phospho-IRS-1 (Ser302) antibody (2384), anti-phospho-IRS-1 (Ser318) antibody (5610), anti-phospho-IRS-1 (Ser612) antibody (2386), anti-phospho-IRS-1 (Ser636/639) antibody (2388), anti-phospho-IRS-1 (Ser1101) antibody (2385), anti-mTOR antibody (2972), anti-phospho-mTOR (Ser2448) antibody (2971), anti-PARP antibody (9542), anti-Raptor antibody (2280), anti-Rictor antibody (2140), anti-phospho-p70 S6K (Thr389) antibody (9234), anti-phospho-S6 (Ser240/Ser244) antibody (2215), anti-S6 antibody (2317), and anti-TSC2 antibody (4308) were purchased from Cell Signaling Technologies. Anti-HSP90 antibody (sc-7947), anti-IRS-2 antibody (sc-8299), anti-p70 S6K antibody (sc-230) and anti-ubiquitin antibody (P4D1) (sc-8017) were purchased from Santa Cruz Biotechnology. Anti-FLAG antibody (clone M2) (F1804), anti-α-tubulin antibody (clone DM1A) (T9026), and anti-phospho-Tyr antibody (clone 4G10) (05-777) were purchased from Sigma-Aldrich. Anti-IRS-1 antibody (06-248), anti-phospho-IRS-1 (Ser307) antibody (07-247), anti-p85 antibody (06-195), and anti-Myc antibody (05-419) were purchased from EMD Millipore. IRS-1 polyclonal antibody for immunoprecipitation was raised in rabbit as previously described (Fukushima et al., 2011).

Plasmids

A complete list of the plasmids used in this study is available in Table S1. Point

mutations in the indicated plasmids were introduced by site-directed mutagenesis using PrimeSTAR Mutagenesis Basal Kit (Takara Bio Inc., Shiga, Japan) and confirmed by Sanger sequencing. A series of IRS-1 deletion mutants (amino acid residues 1–865, 1–542, 1–259 and full-length of rat IRS-1) were cloned into pFLAG-CMV vector. The full-length IRS-1 cDNA was also cloned into pCMV5-Myc vector. The cDNAs encoding human SOCS3 (kindly provided by K. Ueki, The University of Tokyo, Japan), human Cullin1, human Cullin7, and human Fbxw8 (kindly provided by R. J. Smith, Brown University, USA) were subcloned into pFLAG-CMV vector. β-TRCP1 and β-TRCP2 were cloned by RT-PCR using total RNA isolated from HEK293T cells and subcloned into pFLAG-CMV vector. Mdm2 and Raptor were cloned by RT-PCR using total RNA isolated from L6 cells and subcloned into pFLAG-CMV vector. Fbxo40 was cloned by RT-PCR using total RNA isolated from rat gastrocnemius muscle and subcloned into pFLAG-CMV vector. The cDNA of GFP amplified from pEGFP-C1 was subcloned into pFLAG-CMV vector. pcDNA3.1-FLAG-mTOR^{SL1+IT} was previously described (Ohne et al., 2008). The full-length and deletion mutants of FLAG-IRS-1 for retroviral expression were generated by PCR and subcloned into pMXs-Puro vector. To generate pMXs-Puro-FLAG-IRS-1 STA (301-600), the partial fragment of IRS-1 mutant, which harbors the substitution of possible Ser/Thr residues into Ala in the region corresponding to amino acid residues 301-600, was synthesized by GeneArt Strings DNA fragment service (Thermo Fisher Scientific where?), and fused with other IRS-1 regions and N-terminal FLAG epitope to assemble into pMXs-Puro by In-Fusion HD Cloning kit (Takara Bio Inc., Shiga, Japan). pMXs-Puro-FLAG-IRS-1 STA (301-500) and STA (501-600) were generated by PCR of the corresponding mutated region and other parts of FLAG-IRS-1 followed by In-Fusion-mediated assembly into pMXs-Puro. TSC2 was cloned by RT-PCR using total RNA isolated from L6 cells and subcloned into pMXs-Puro vector. For the bacterial expression, the partial region of IRS-1 corresponding to amino acid residues 256-443 was subcloned into pGEX-5X-3. 4EBP1 was cloned by RT-PCR using total RNA isolated from L6 cells and subcloned into pGEX-4T-1 vector.

Cell culture and transfection

L6 and HEK293T cells were cultured in Dulbecco's modified Eagle's medium (DMEM) supplemented with 10% fetal bovine serum (FBS) in a 5% CO_2 incubator.

DMEM containing 4.5 g/l of glucose (Nissui Seiyaku Co., Tokyo, Japan) was used. L6 cells were maintained in the undifferentiated myoblast state in either growing or serum-starved condition tested in this study. PLAT-E cells (provided by T. Kitamura, The University of Tokyo, Tokyo, JAPAN) were used for retrovirus packaging. The transfection of expression plasmids in HEK 293T cells was performed by using polyethylenimine (PEI) as previously described (Lanzerstorfer et al., 2015). For RNA interference (RNAi), L6 cells were transfected with siRNAs (RNAi Corp., Tokyo, Japan) listed in Table S2 by using Lipofectamine RNAiMAX (Thermo Fisher Scientific). For Raptor and Rictor knockdown, we performed the two consecutive siRNA transfections at a 48 hr interval to achieve high efficiency of the target gene knockdown.

Isolation of primary embryonic fibroblasts and myoblasts from mice

For primary mouse embryonic fibroblasts (MEFs) isolation, embryos dissected out at E14.5 from pregnant C57BL/6 mice were washed with PBS. The head and visceral tissues were removed from the isolated embryos, and the remaining bodies were minced and then dissociated at 37°C for 20 min in Hanks balanced salt solution (HBSS) supplemented with 0.05% trypsin and 0.01% EDTA. After incubation, DMEM containing 10% FBS was added, and the tissue mixture was then incubated at room temperature for 5 min. The supernatant was transferred into a new tube. Cells were collected by centrifugation (200 *g* for 5 min) and resuspended in the fresh DMEM containing 10% FBS. The cells were grown on the culture dishes at 37°C with 5% CO_2. We used the MEFs within three passages in this study.

For primary mouse myoblasts isolation, 6-week-old C57BL/6 male mice were sacrificed and the hind limb muscles were isolated. After washed with PBS, the isolated muscle tissues were minced and then digested at 37°C for 1 hr in DMEM supplemented with 400 U/ml collagenase II (Worthington Biochemical Corp., Lakewood, NJ). The digested slurry was spun at 1,400 *g* for 5 min at room temperature, and the supernatant was removed. The pelleted muscle tissues were resuspended in DMEM supplemented with 10% FBS followed by pipetting up and down twenty times. The slurry was passed through 70 μm and then 40 μm cell strainers (BD Falcon) followed by centrifugation (1,400 *g* for 5 min). The cell pellets were resuspended in Ham's F-10 Nutrient Mix (Thermo Fisher Scientific) supplemented with 20% FBS and 10 ng/ml human

recombinant basic fibroblast growth factor (bFGF; a kind gift from M. Mori, Takeda Pharmaceutical Company). The cells were grown on the culture dishes coated with Matrigel (Corning) for three days at 37°C with 5% CO_2. To purify myoblast population, the cells were trypsinized, suspended in F-10 supplemented with 20% FBS and 10 ng/ml bFGF, transferred to non-coated culture dish, and then incubated for 45 min at 37°C with 5% CO_2. After the pre-plating, the supernatant cells were grown on the new dishes coated with Matrigel. The pre-plating step was performed every 72 hr three times which achieved over 90% purity of myoblast population as judged by phase contrast microscopy. The myoblasts were cultured in F-10 supplemented with 20% FBS and 10 ng/ml bFGF until reaching 70% confluency.

All animal care and experiments conformed to the Guidelines for Animal Experiments of The University of Tokyo, and were approved by the Animal Research Committee of The University of Tokyo.

Retrovirus production and generation of stable cell lines

PLAT-E cells were transiently transfected with pMXs-Puro vectors by using PEI reagent, and the medium containing retrovirus was collected. L6 cells were incubated with the virus-containing medium supplemented with 2 μg/ml of polybrene. Uninfected cells were removed by puromycin selection.

Generation of TSC2 knockout L6 cell lines using the CRISPR-Cas9 system

To allow the selection of cells transfected with guide RNA-Cas9 construct, pCS2-U6-gRNA-FN-Cas9-N-P2A-Puro was generated as follows. SpCas9 fused with N-terminal FLAG-NLS and C-terminal NLS (FN-Cas9-N) was amplified from pCAG-T3-hCAS-pA (Addgene plasmid #48625, kindly provided by W. Fujii, The University of Tokyo, Tokyo, Japan) and subcloned into pCS2-FLAG vector (kindly provided by M. Taira, The University of Tokyo, Tokyo, Japan). Puromycin resistance gene (Puro) was fused to the C-terminus of FN-Cas9-N with a self-cleaved sequence P2A (Kim et al., 2011) using In-Fusion HD Cloning kit. In addition to FN-Cas9-N-P2A-Puro, which is driven by CMV promoter, the guide RNA expression cassette consisted of U6 promoter and single guide RNA (sgRNA) scaffold (Ran et al., 2013) was synthesized by GeneArt Strings DNA fragment service, and cloned into the same plasmid. The guide sequences targeting exon 2 of rat *Tsc2* were designed using

the CRISPR design tool (http://www.genome-engineering.org/crispr) and cloned into pCS2-U6-gRNA-FN-Cas9-N-P2A-Puro. The sgRNA sequences used in this study are the following: 5'-GTATTAGGACTGGGAACGTCA-3' for clone #1; 5'-GTTCAAGATACTATTAGGAC-3' for clone #2. L6 cells were transfected with the constructs using Lipofectamine LTX reagent (Thermo Fisher Scientific) according to the manufacturer's instructions. 24 hr post transfection, untransfected cells were removed by puromycin selection for 72 hr. Single clones were isolated by dilution cloning, expanded in the absence of puromycin and screened for TSC2 by immunoblotting. Genomic DNA was purified from the clones, and the region including sgRNA target sites in exon 2 was amplified with PrimeSTAR Max DNA Polymerase (Takara Bio Inc., Shiga, Japan) using the following primers: Tsc2 forward, 5'-CGGTACCCGGGGATCTCATCATGGCTCTGTTCACCC-3'; Tsc2 reverse, 5'-CGACTCTAGAGGATCGCTGTCCTGAAACTCACTTTG-3'. PCR products were cloned into pUC19 vector by using In-Fusion HD Cloning kit. To determine the indels of individual alleles, the plasmids from at least 8 bacterial colonies were analyzed by Sanger sequencing. L6 cell clones transfected with Cas9 only plasmid were used as negative control.

Cell stimulation

Recombinant human IGF-I was kindly donated by T. Ohkuma (Astellas Pharma Inc., Tokyo, Japan). Prior to ligand stimulation, L6 cells and MEFs were serum-starved for 12 hr in DMEM supplemented with 0.1% bovine serum albumin (BSA), and then treated with the ligand (100 ng/ml IGF-I) for the indicated time. For ligand stimulation, primary myoblasts were serum-starved for 6 hr in DMEM supplemented with 0.1% bovine serum albumin (BSA). When needed, cells were preincubated for 30 min with chemical inhibitors at the following concentrations: 100 nM Torin1 (Cayman Chemical), 100 nM rapamycin (Sigma-Aldrich), 25 μM PF-4708671 (Cayman Chemical), 5 or 25 μM MG-132 (EMD Millipore), and 1 or 5 μM lactacystin (Enzo Life Sciences). For amino acid stimulation, L6 cells were washed twice with HBSS followed by incubation with amino acid free DMEM (4.5 g/l glucose; Wako Pure Chemical Industries, Osaka, Japan) for 2 hr, and then stimulated by replacing medium to amino acid containing DMEM (4.5 g/l glucose; Nissui Seiyaku Co., Tokyo, Japan) for the indicated time.

Immunoprecipitation and immunoblotting

After the indicated treatment, cells were rinsed once with ice-cold PBS and then lysed with lysis buffer A (25 mM Tris-HCl, pH 7.4, 150 mM NaCl, 1 mM EDTA, 10% glycerol, 1% Triton X-100, 100 Kallikrein inhibitor units [KIU]/ml aprotinin, 20 μg/ml phenylmethylsulfonyl fluoride [PMSF], 10 μg/ml leupeptin, 5 μg/ml pepstatin A, 500 μM Na_3VO_4, and 10 mg/ml *p*-nitrophenyl phosphate [PNPP]). After brief sonication, the clear supernatant was obtained by centrifugation at 15,000 *g* for 15 min at 4°C. For immunoprecipitation of IRS-1, the lysates were incubated with anti-IRS-1 antibody overnight at 4°C, and further incubated in the presence of Protein G Sepharose beads (GE Healthcare). For immunoprecipitation of FLAG fusion proteins, the lysates were incubated with Anti-FLAG M2 affinity gel beads or IgG-Agarose beads (Sigma-Aldrich) for 2 hr. For analysis of the mTORC1-IRS-1 complex, immunoprecipitation was performed with lysis buffer B (40 mM Hepes-KOH, pH 7.5, 120 mM NaCl, 1 mM EDTA, 0.3% CHAPS, 50 mM NaF, 10 mM β-glycerophosphate, 100 Kallikrein inhibitor units [KIU]/ml aprotinin, 20 μg/ml PMSF, 10 μg/ml leupeptin, 5 μg/ml pepstatin A, 500 μM Na_3VO_4, and 10 mg/ml PNPP) to maintain the mTOR complex as described previously (Kim et al., 2002). Immunoprecipitates were collected by centrifugation and washed four times with lysis buffer, and then proteins were eluted with Laemmli's sample buffer. Samples were then separated by SDS-PAGE and transferred to Immobilon-P polyvinylidene difluoride (PVDF) membrane (EMD Millipore). Immunoblotting was performed with the indicated antibodies and visualized with Western Lightning Plus-ECL substrate (PerkinElmer). Quantification of immunoblots was performed by using ImageJ software. Densitometry was performed in the linear phase of the exposure.

Mass spectrometry

Liquid chromatography/tandem mass spectrometry (LC-MS/MS) was performed as previously described (Natsume et al., 2002).

Ubiquitination assay

After the indicated treatment, cells were washed with ice-cold PBS and then lysed with lysis buffer A supplemented with 100 mM *N*-ethylmaleimide (NEM). The cleared lysates were subjected to immunoprecipitation with Anti-FLAG M2 affinity gel beads.

The immunoprecipitates were then washed three times with lysis buffer A supplemented with 100 mM NEM, and heated in 50 mM Tris-HCl, pH 7.4, 150 mM NaCl, and 1% SDS at 98°C for 5 min to disrupt non-covalent protein-protein interactions. The supernatants diluted with lysis buffer A (1:10) were re-immunoprecipitated with Anti-FLAG M2 affinity gel beads, and then subjected to SDS-PAGE. After transfer to PVDF membranes, the membranes were subjected to a denaturing treatment prior to blocking the primary antibody by incubation for 30 min at 4°C in 50 mM Tris-HCl, pH 7.5, 6M guanidine-HCl, and 5 mM 2-mercaptoethanol.

***In vitro* dephosphorylation**

The cell lysates were prepared using lysis buffer A without phosphatase inhibitors (Na_3VO_4 and PNPP). For dephosphorylation of cell lysates, 20-30 μg of total lysate protein was incubated with 1 unit/ μg of protein of calf intestine alkaline phosphatase (CIP; Takara Bio Inc., Shiga, Japan). For dephosphorylation of immunoprecipitated proteins, the immunoprecipitates from a 60-mm culture dish were incubated with 30–50 units of CIP. After incubation for 60 min at 37°C, the reaction was quenched by adding Laemmli's sample buffer and heating samples. The samples were subsequently analyzed by immunoblotting with the indicated antibodies.

Preparation of recombinant protein

Escherichia coli BL21 were transformed with pGEX-4T-1, pGEX-IRS-1 (256-443), or pGEX-4EBP1, and grown in LB supplemented with ampicillin at 25°C to OD_{600} of 0.7. Expression of GST and GST-4EBP1 was induced with 0.2 mM isopropyl β-$_D$-thiogalactopyranoside (IPTG) at 25°C overnight. For expression of GST-IRS-1 (256-443), cells were grown without IPTG at 25°C overnight. The cells were harvested by centrifugation and homogenized with a sonicator in a buffer of PBS containing 1% Triton X-100. The proteins were purified by using glutathione Sepharose 4 fast flow (GE Healthcare), and eluted with a buffer of 50 mM Tris-HCl, pH 8.0, 300 mM NaCl, 20 mM glutathione, and 1 mM dithiothreitol. The purified proteins were subjected to SDS-PAGE followed by Coomassie brilliant blue (CBB) staining to check the purity.

***In vitro* mTOR kinase assay**

HEK293T cells expressing FLAG-GFP or FLAG-mTOR SL1+IT (Ohne et al., 2008)

were lysed with lysis buffer B, and the lysates were subjected to immunoprecipitation with Anti-FLAG M2 affinity gel beads. The beads were then washed with kinase wash buffer (10 mM Hepes-KOH, pH 7.4, 50 mM NaCl, and 50 mM β-glycerophosphate). Kinase assay was performed in 40 μl of kinase buffer (10 mM Hepes-KOH, pH 7.4, 50 mM NaCl, 50 mM β-glycerophosphate, 10 mM $MgCl_2$, 4 mM $MnCl_2$, and 250 μM ATP) containing 1 μg of GST, GST-IRS-1 (256-443), or GST-4EBP1, and the mixtures were incubated for 10 or 30 min at 30°C. Reactions were quenched by adding Laemmli's sample buffer and heating samples. The samples were subsequently analyzed by immunoblotting with the indicated antibodies.

RT-PCR analysis

Total RNA from L6 cells and primary myoblasts was extracted with TRIzol reagent (Thermo Fisher Scientific). First-strand cDNA was synthesized with ReverTra Ace qPCR Master Mix with gDNA Remover (TOYOBO, Osaka, Japan). Quantitative PCR was performed with THUNDERBIRD SYBR qPCR Mix (TOYOBO, Osaka, Japan) on an ABI StepOnePlus Real Time PCR System (Applied Biosystems). To normalize the relative expression, a standard curve was prepared for each gene for relative quantification, and the expression level of each gene was normalized to the *Gapdh* or *Rn18s* gene indicated in the figure legends. Specific primers described below were used:
Cul7 F 5'-ATGTGTACCGGAAGTACGGC-3' and
Cul7 R 5'-GATGGGGGATCTTGGGCTTC-3';
Fbxw8 F 5'-TTCTCACGATGGAGTTGTCATCG-3' and
Fbxw8 R 5'-TGAGCGCAAGGGCTTGTATTC-3';
Btrc F 5'-AAGCGTGGTATCGCCTGTTT-3' and
Btrc R 5'-ATGCACCGCACTCTATGTCC-3';
Fbxw11 F 5'-TAGAGGGGCACGAAGAGTTGG-3' and
Fbxw11 R 5'-AAGAGCAGCCTGCAAATCCCAG-3';
Gapdh F 5'-TCTCTGCTCCTCCCTGTTCTA-3' and
Gapdh R 5'-GGTAACCAGGCGTCCGATAC-3';
Rn18s F 5'-TCCCAGTAAGTGCGGGTCATA-3' and
Rn18s R 5'-CGAGGGCCTCACTAAACCATC-3'.
RT-PCR for mouse myoblast markers as well as *Gapdh* mRNA was performed with Ex Taq polymerase (Takara Bio Inc., Shiga, Japan) and specific primers described below:

Myod1 F 5'-CGGCAGAATGGCTACGACAC-3' and
Myod1 R 5'-ATCGCATTGGGGTTTGAGCC-3';
Pax7 F 5'-TCAAGCCAGGAGACAGCTTG-3' and
Pax7 R 5'-TAGGCTTGTCCCGTTTCCAC-3';
Gapdh F 5'-AAGGTCATCCCAGAGCTGAA-3' and
Gapdh R 5'-CTGCTTCACCACCTTCTTGA-3'.
The samples were subjected to 2% agarose electrophoresis followed by ethidium bromide staining to visualize the PCR products.

DNA synthesis assay

10,000 L6 cells grown on 48-well plates were serum-starved for 12–14 hr followed by the stimulation with or without IGF-I for 12 hr. [Methyl-^{3}H]thymidine (0.3 mCi/well; GE Healthcare) was added to each well 4 hr before the termination of each experiment. The incorporation was quenched by adding ice-cold 1M ascorbic acid. The cells were rinsed twice with PBS and twice with 10% trichloroacetic acid. The acid-precipitated materials were solubilized in 0.2 N NaOH and 0.1% SDS, and then mixed into Clear-sol II (nacalai tesque, Kyoto, Japan). The radioactivity was measured by a liquid scintillation counter.

Flow cytometric analysis for apoptosis

L6 cells grown to confluence were rinsed once with HBSS and then switched to serum-free medium (DMEM supplemented with 0.1% BSA) with or without IGF-I (20 ng/ml) for 6 hr. The adherent cells were detached using Accutase (nacalai tesque, Kyoto, Japan), and both floating and adherent cells were collected by centrifugation. For detection of apoptosis, they were co-stained with Annexin V-FITC (Thermo Fisher Scientific) and 7-AAD (Biolegend) according to the manufacturer's instruction. Stained cells were subjected to the flow cytometric analysis using BD FACSVerse (BD Biosciences).

Multiple sequence alignment

Multiple sequence alignment for analysis of β-TRCP binding site in IRS proteins was performed using Clustal X 2.1 (Larkin et al., 2007). The sequences analyzed are as follows: human IRS-1 (*Homo sapiens*, NP_005535.1), rat IRS-1 (*Rattus norvegicus*,

NP_037101.1), mouse IRS-1 (*Mus musculus*, NP_034700.2), zebrafish IRS-1 (*Danio rerio*, XP_687702.4), human IRS-2 (*Homo sapiens*, NP_003740.2), rat IRS-2 (*Rattus norvegicus*, NP_001162104.1), and mouse IRS-2 (*Mus musculus*, NP_001074681.1).

Statistical analysis

Comparisons between more than two groups were analyzed by analysis of variance (ANOVA) and the Tukey *post hoc* test. *P* values of <0.05 were considered statistically significant. All statistical analyses were performed with EZR (Kanda, 2013), which is a graphical user interface for R (The R Foundation for Statistical Computing, Vienna, Austria).

References

Fukushima, T., Arai, T., Ariga-Nedachi, M., Okajima, H., Ooi, Y., Iijima, Y., Sone, M., Cho, Y., Ando, Y., Kasahara, K., Ozoe, A., Yoshihara, H., Chida, K., Okada, S., Kopchick, J.J., Asano, T., Hakuno, F., and Takahashi, S.-I. (2011). Insulin receptor substrates form high-molecular-mass complexes that modulate their availability to insulin/insulin-like growth factor-I receptor tyrosine kinases. Biochem. Biophys. Res. Commun. 404, 767–773.

Kanda, Y. (2013). Investigation of the freely available easy-to-use software "EZR" for medical statistics. Bone Marrow Transplant. 48, 452–458.

Kim, J.H., Lee, S.-R., Li, L.-H., Park, H.-J., Park, J.-H., Lee, K.Y., Kim, M.-K., Shin, B.A., and Choi, S.-Y. (2011). High cleavage efficiency of a 2A peptide derived from porcine teschovirus-1 in human cell lines, zebrafish and mice. PLoS One 6, e18556.

Larkin, M.A., Blackshields, G., Brown, N.P., Chenna, R., McGettigan, P.A., McWilliam, H., Valentin, F., Wallace, I.M., Wilm, A., Lopez, R., Thompson, J.D., Gibson, T.J., and Higgins, D.G. (2007). Clustal W and Clustal X version 2.0. Bioinformatics 23, 2947–2948.

Natsume, T., Yamauchi, Y., Nakayama, H., Shinkawa, T., Yanagida, M., Takahashi, N., and Isobe, T. (2002). A direct nanoflow liquid chromatography-tandem mass spectrometry system for interaction proteomics. Anal. Chem. 74, 4725–4733.

Ohne, Y., Takahara, T., Hatakeyama, R., Matsuzaki, T., Noda, M., Mizushima, N., and Maeda, T. (2008). Isolation of hyperactive mutants of mammalian target of rapamycin. J. Biol. Chem. 283, 31861–31870.

Ran, F.A., Hsu, P.D., Wright, J., Agarwala, V., Scott, D.A., and Zhang, F. (2013). Genome engineering using the CRISPR-Cas9 system. Nat. Protoc. 8, 2281–2308.